Destruction of ^{7}Be in big bang nucleosynthesis via long-lived sub-strongly interacting massive particles as a solution to the Li problem

Masahiro Kawasaki[1,2] and Motohiko Kusakabe[1,*]

[1]*Institute for Cosmic Ray Research, University of Tokyo, Kashiwa, Chiba 277-8582, Japan*
[2]*Institute for the Physics and Mathematics of the Universe, University of Tokyo, Kashiwa, Chiba 277-8582, Japan*
(Received 14 December 2010; revised manuscript received 30 January 2011; published 18 March 2011)

We identify reactions which destroy ^{7}Be and ^{7}Li during big bang nucleosynthesis (BBN) in the scenario of BBN catalyzed by a long-lived sub-strongly-interacting massive particle (sub-SIMP or X particle). The destruction associated with nonradiative X captures of the nuclei can be realized only if the interaction strength between an X particle and a nucleon is properly weaker than that between two nucleons to a degree depending on the mass of X. Binding energies of nuclei to an X particle are estimated taking the mass and the interaction strength to nuclei of the X as input parameters. Nuclear reaction rates associated with the X are estimated naively and adopted in calculating evolutions of nuclear abundances. We suggest that the ^{7}Li problem, which might be associated with as-yet-unrecognized particle processes operating during BBN, can be solved if the X particle interacts with nuclei strongly enough to drive ^{7}Be destruction but not strongly enough to form a bound state with ^{4}He of relative angular momentum $L = 1$. Justifications of this scenario by rigorous calculations of reaction rates using quantum mechanical many-body models are highly desirable since this result involves many significant uncertainties.

DOI: 10.1103/PhysRevD.83.055011 PACS numbers: 26.35.+c, 95.35.+d, 98.80.Cq, 98.80.Es

I. INTRODUCTION

The standard big bang nucleosynthesis (BBN) model predicts primordial light element abundances which are more or less consistent with abundances inferred from observations of old distant astronomical objects. Deviations from the standard BBN (SBBN) model are, therefore, constrained if predicted abundances in theoretical models change from those in the SBBN. Constraints on the existence of long-lived exotic particles which interact with nuclei by strong force [1–4] or Coulomb force [5–22] have been derived as well as those on the decay of long-lived exotic particles into standard model particles which have electromagnetic or hadronic interactions [23–50].

A prominent problem relating to the abundances predicted in the SBBN model and inferred from observations is lithium problem [51,52]. Primordial lithium abundances are inferred from measurements in metal-poor halo stars (MPHSs). Observed abundances are roughly constant as a function of metallicity [51–57] at $^7\mathrm{Li/H} = (1\text{–}2) \times 10^{-10}$. The theoretical prediction by the SBBN model is, however, a factor of 2–4 higher, e.g., $^7\mathrm{Li/H} = (5.24^{+0.71}_{-0.67}) \times 10^{-10}$ [58], when its only parameter, the baryon-to-photon ratio, is deduced from the observation with Wilkinson Microwave Anisotropy Probe (WMAP) of the cosmic microwave background (CMB) radiation [59]. This discrepancy indicates some mechanism of ^{7}Li reduction having operated in some epoch from the BBN to this day. One possible astrophysical process to reduce ^{7}Li abundances in stellar surfaces is the gravitational settling in the model including a combination of the atomic and turbulent diffusion [60,61]. The precise trend of Li abundance as a function of effective temperature of stars in the metal-poor globular cluster NGC 6397 is, however, not reproduced theoretically [62].

^{6}Li/^{7}Li isotopic ratios of MPHSs have also been measured spectroscopically. The ^{6}Li abundance as high as $^6\mathrm{Li/H} \sim 6 \times 10^{-12}$ was suggested [52], which is about 1000 times higher than the SBBN prediction [63]. Convective motions in the atmospheres of MPHSs could cause systematic asymmetries in the observed line profiles and mimic the presence of ^{6}Li [65]. A few or several MPHSs, however, have high ^{6}Li abundances larger than levels caused by this effect [66]. This high ^{6}Li abundance is a problem since the standard Galactic cosmic ray nucleosynthesis models predict negligible amounts of ^{6}Li yields compared to the observed level in the epoch corresponding to the metallicity of the stars, i.e., $[\mathrm{Fe/H}] < -2$ [67,68].

The possibility that the ^{7}Li and ^{6}Li problems stem from uncertainties in nuclear reactions used in theoretical BBN calculation is unlikely [69] unless there remain to be observed new resonant states contributing to ^{7}Be destruction [70,71]. The ^{7}Li reduction needs a destruction mechanism of ^{7}Be during or after BBN and before stellar activities since the ^{7}Li nuclei observed in MPHSs are thought to have originated from the electron capture process of ^{7}Be which is produced in the BBN.

Some particle models beyond the standard model include heavy ($m \gg 1$ GeV) long-lived colored particles. The scenarios, i.e., split supersymmetry [72,73], weak scale supersymmetry with a long-lived gluino [74–76] or squark [77] as the next-to-lightest supersymmetric particles, and extended theories with new kinds of colored particles [78,79], may be tested in experiments such as

*kusakabe@icrr.u-tokyo.ac.jp

the Large Hadron Collider. The heavy colored particles would be confined at temperatures below the deconfinement temperature $T_C \sim 180$ MeV inside exotic heavy hadrons, i.e., strongly-interacting massive particles (SIMPs) which we call X particles [80]. Their thermal relic abundances after the freeze-out of annihilations depend on the annihilation cross sections, and theoretical estimates predict various values which extend over more than several order of magnitude at the heavy mass limit [81].

If the annihilation cross section is not different from a typical value for strong interaction, i.e., $\sigma \sim \mathcal{O}(\mathrm{GeV}^{-1})^2$, however, the final abundance of X particles can be derived under the assumption that their abundances are fixed when the annihilation rate becomes smaller than the Hubble expansion rate of the universe [80]. The relic abundance can then be written

$$\frac{N_X}{s} \sim \sqrt{\frac{15}{\pi}} \frac{g_*^{1/2}}{g_{*s}} \frac{m^{1/2}}{\sigma T_B^{3/2} m_{\mathrm{Pl}}}, \tag{1}$$

where N_X is the number density of the X particle, $s = 2\pi^2 g_{*s} T^3/45$ is the entropy density with $g_{*s} \sim 10$ the total number of effective massless degrees of freedom in terms of entropy [82] just below the QCD phase transition, g_* is the total number of effective massless degrees of freedom in terms of number [82], m is the mass ($m \gg 1$ GeV) of the heavy long-lived colored particles, σ is the annihilation cross section of the X particle, T_B is the temperature of the universe at which the X particles are formed, and m_{Pl} is the Planck mass. The number abundance of the X's with respect to that of baryons is then

$$\frac{N_X}{n_b} \sim 0.5 \times 10^{-8} \left(\frac{g_*}{10.75}\right)^{1/2} \left(\frac{m}{\mathrm{TeV}}\right)^{1/2} \left(\frac{T_B}{180\,\mathrm{MeV}}\right)^{-3/2} \times \left(\frac{\sigma}{m_\pi^{-2}}\right)^{-1}, \tag{2}$$

where n_b is the number density of baryons, and $m_\pi \sim 140$ MeV is the mass of pion. The thermal relic abundance is inversely proportional to the annihilation cross section which depends on the particle theory. In addition, there might be a nonthermal production of long-lived colored particles which is not directly related to the thermal production. The final abundance of the X is, therefore, uncertain. So we consider the X abundance as a free parameter in this paper.

Observational constraints on hypothetical SIMPs have been studied [83–85]. Effects of exotic neutral stable hadrons on BBN were studied in Ref. [1]. The authors assumed that the strong force between a nucleon and an exotic hadron (X) is similar to that between a nucleon N and a Λ hyperon. In addition, new hadrons are assumed to be captured in a bound state of ^{4}He plus X after BBN. Based upon an analytic estimation, they suggested that beryllium has the largest number fraction A_X/A of bound states with the hadrons among the light elements produced in BBN, where the A and A_X are a nuclide A and a bound state of A with a hadron X. Mohapatra and Teplitz [3] estimated the cross section of X capture by ^{4}He and suggested that a large fraction of free X particles would not become bound into light nuclides and remain free contrary to the previous suggestion [1]. In deriving the result of those two studies, it has been assumed that exotic hadrons interact with normal nuclei by typical strengths of strong interaction and implicitly assumed that its mass is about that of Λ hyperon, i.e., $m_X \sim 1.116$ GeV [86].

Effects on BBN of long-lived exotic hadrons of $m \gg 1$ GeV have been studied recently [4]. The authors have assumed that the interaction strength between an X particle and a nucleon is similar to that between nucleons. Rates of many reactions associated with the X particle were estimated, and a network calculation of the nucleosynthesis including effects of the X was performed. The constraint on the decay lifetime of such X particles, i.e., $\tau_X \lesssim 200$ s was derived from a comparison of calculated abundances with observational abundance constraints of light elements.

Two interesting predictions of the model [4] are signatures of the X particles on primordial abundances which should be seen in future astronomical observations: 1) ^{9}Be and B can be produced in amounts more than predicted in the SBBN. Future observations of Be and B abundances in MPHSs may show primordial constant values originating from the BBN catalyzed by the X particle. 2) The isotopic ratio $^{10}\mathrm{B}/^{11}\mathrm{B}$ tends to be very high. This is different from predictions of other models for boron production, i.e., the cosmic ray nucleosynthesis ($^{10}\mathrm{B}/^{11}\mathrm{B} \sim 0.4$ [87–89]) or the supernova neutrino process ($^{10}\mathrm{B}/^{11}\mathrm{B} \ll 1$ [90,91]). They concluded that the ^{6}Li or ^{7}Li problems is not solved under their assumption.

Since interactions between long-lived exotic hadrons X and a nucleon are not known as well as their masses, we are investigating effects of such particles in various cases of interaction strengths and masses. We found on the way a new possibility that reactions associated with the X particle reduce ^{7}Be abundance and that the ^{7}Li problem is solved.

In this paper, we report details of the destruction mechanism of ^{7}Be in the presence of the X particle. We carry out a network calculation of BBN in the presence of a long-lived SIMP X^0 of a zero charge taking the mass and the strength of interaction with a nucleon as characterizing parameters. In Sec. II, assumptions on the X^0 particle, estimations for binding energies between nuclei and an X^0, and rates of important reactions are described. Effects of the X^0 decay inside X nuclei are not considered in our model. They should be addressed in the future. In Sec. III, the destruction processes of ^{7}Be and ^{7}Li are identified. With results of the network calculations of BBN, we delineate the parameter region in which the ^{7}Be and ^{7}Li destructions possibly operate. If the X^0 particle interacts with nuclei strongly enough to drive ^{7}Be destruction but not strongly enough to form a bound state with ^{4}He

of relative angular momentum $L = 1$, then it might solve the ^{7}Li problem of standard BBN. In Sec IV, conclusions of this work are summarized and this model for ^{7}Li reduction is compared with other models.

II. MODEL

A strongly-interacting massive particle (SIMP) X of spin zero and charge zero is assumed to exist during the epoch of BBN. Its mass is one parameter since it is not known *a priori* at the moment. Two types of nuclear potentials between an X^0 and a nucleon (XN) are considered in this study. One is the Gaussian type given by

$$v(r) = v_0 \delta \exp[-(r/r_0)^2], \tag{3}$$

where $v_0 = -72.15$ MeV and $r_0 = 1.484$ fm [92], and the interaction strength is varied by changing δ, the second parameter. When the δ equals unity then the binding energy of deuteron, i.e., 2.224 MeV is obtained.

The potential between an X^0 and a nuclide A (XA) is given by

$$V(r) = \int v(\boldsymbol{x}) \rho(\boldsymbol{r}') d\boldsymbol{r}', \tag{4}$$

where $\boldsymbol{r}$ is the radius from an X to the center of mass of A, $\boldsymbol{r}'$ is the distance between the center of mass of A and a nucleon inside the nuclide A, $\boldsymbol{x} = \boldsymbol{r} + \boldsymbol{r}'$ is the distance between the X and the nucleon, and $\rho(\boldsymbol{r}')$ is the nucleon density of the nucleus which is generally distorted by potential of an X^0 from the density of normal nucleus. Under the assumption of spherical symmetry in nucleon density, i.e., $\rho(r)$, the potential is written in the form of

$$V(r) = \pi v_0 \delta \frac{r_0^2}{r} \int_0^\infty dr' r' \rho(r') \times \left\{ \exp\left[-\frac{(r - r')^2}{r_0^2} \right] - \exp\left[-\frac{(r + r')^2}{r_0^2} \right] \right\}. \tag{5}$$

Another potential is a well given by

$$v_{\rm w}(r) = v_{0\rm w} \delta_{\rm w} \qquad (\text{for } 0 \le r < r_{0\rm w}), \tag{6}$$

and $v_{\rm w}(r_{0\rm w} \le r) = 0$. Parameters are fixed to be $v_{0\rm w} = -20.06$ MeV and $r_{0\rm w} = 2.5$ fm. In order to make a comparison between the two potential cases easy, integrals, i.e., $I = \int v(r) d\boldsymbol{r}$ for both cases are made equal when $\delta = \delta_{\rm w} = 1$. This integral is a characteristic quantity which is related to binding energies. The requirement of equal integral values and an assumption of $r_{0\rm w} = 2.5$ fm [95] leads to

$$v_{0\rm w} = v_0 \frac{3\sqrt{\pi}}{4} \left(\frac{r_0}{r_{0\rm w}} \right)^3 = -20.06 \text{ MeV}. \tag{7}$$

The XA potential is given by

$$V(r)_{\rm w} = 2\pi v_{0\rm w} \delta_{\rm w} \frac{1}{r} \int_0^\infty dr' r' \rho(r') \int_{|r-r'|}^{r+r'} dx x H(x - r_{0\rm w}), \tag{8}$$

where $H(x)$ is the Heaviside step function.

As a crude assumption, the nucleon density $\rho(r)$ is approximately given by the undistorted one for normal nucleus. The folding technique to derive XA potential from the XN potential [Eq. (4)] then does not exactly yield the XA potential in any mathematically-rigorous method of calculation. In order to derive precise results of nuclear structures or energy levels, all nucleons as well as an X^0 and all interactions among them need to be taken into account with many-body quantum mechanical calculations. Since such calculations are unrealistically difficult, three or four-body models for an X^0 particle and nuclear clusters composing the nucleus should be utilized as were done in the case of hypernuclei [96]. The assumption taken here only provides some reasonable estimate of what an effective X-nucleus reaction might look like with all the nuclear degrees of freedom frozen out. The folding procedure, however, might produce a more useful approximation than in the nuclear case since the X^0 does not participate in the Pauli principle among nucleons.

The nucleon density of nuclei with mass number $A \ge 2$ is assumed to be Gaussian, i.e,

$$\rho(r) = \rho(0) \exp[-(r/b)^2], \tag{9}$$

where $\rho(0) = A\pi^{-3/2} b^{-3}$ is the nucleon density at $r = 0$ and satisfies the normalization $\int \rho(r) d\boldsymbol{r} = A$, with A the mass number. The parameter for the width of density, i.e., b, is related to the root mean square (RMS) nuclear matter radius, which should be determined from experiments, i.e., $b = \sqrt{2/3} r_{\rm m}^{\rm RMS}$.

The XA potential in the case of the Gaussian XN potential, i.e., Eq. (5), is then simply written as

$$V(r) = \frac{v_0 \delta A r_0^3}{(r_0^2 + b^2)^{3/2}} \exp\left(-\frac{r^2}{r_0^2 + b^2} \right). \tag{10}$$

A. Nuclear binding energies

The BBN catalyzed by the X particle is significantly sensitive to binding energies of nuclei to an X^0 particle (X nuclei). The binding to X particles changes the relative energies of initial and final states and may even change the sign of the Q value. [4]. Binding energies and eigenstate wave functions of X nuclei are computed taking into account the nuclear interaction only. The Coulomb interaction between nuclei and the X^0 particle is not included since we assume that the X^0 has a zero charge. The potential is supposed to be spherically symmetric. We solve the two-body Shrödinger equation by a variational calculation using the Gaussian expansion method [97], and obtain binding energies.

TABLE I. Binding energies of X particles to nuclei

nuclide	$r_{\rm m}^{\rm RMS}$ (fm)[a]	References	$E_{\rm Bind}$ (MeV) $\delta = 0.1$	$\delta = 0.2$
${}^1{\rm n}_X$	...	...	...	...
${}^1{\rm H}_X$	...	...	...	...
${}^2{\rm H}_X$	1.971 ± 0.005	[98]	...	0.367
${}^3{\rm H}_X$	1.657 ± 0.097[b]	[99]	0.688	4.39
${}^3{\rm He}_X$	1.775 ± 0.034[b]	[99]	0.569	3.85
${}^4{\rm He}_X$	1.59 ± 0.04	[100]	2.73	9.81
${}^5{\rm He}_X$	2.52 ± 0.03[c]	[100]	1.95	6.39
${}^6{\rm He}_X$	2.52 ± 0.03	[100]	3.14	9.02
${}^5{\rm Li}_X$	2.35 ± 0.03[d]	[100]	2.33	7.48
${}^6{\rm Li}_X$	2.35 ± 0.03	[100]	3.70	10.5
${}^7{\rm Li}_X$	2.35 ± 0.03	[100]	5.14	13.6
${}^6{\rm Be}_X$	2.33 ± 0.02[e]	[100]	3.77	10.7
${}^7{\rm Be}_X$	2.33 ± 0.02	[100]	5.23	13.8
${}^8{\rm Be}_X$	2.33 ± 0.02[e]	[100]	6.74	17.0
${}^9{\rm Be}_X$	2.38 ± 0.01	[100]	7.92	19.4
${}^9{\rm B}_X$	2.45 ± 0.10[f]	[101]	7.45	18.2
${}^4{\rm He}_X^*$	1.59 ± 0.04	[100]	...	2.28
${}^8{\rm Be}_X^*$	2.33 ± 0.02[e]	[100]	3.02	11.1

[a]Root mean square (RMS) nuclear matter radius.
[b]Derived by $(r_{\rm m}^{\rm RMS})^2 = (r_{\rm c}^{\rm RMS})^2 - (a_p^{\rm RMS})^2$ with $a_p^{\rm RMS} = 0.875 \pm 0.007$ fm using a RMS proton matter radius determined in experiment as a RMS charge radius.
[c]Taken from ^{6}He radius.
[d]Taken from ^{6}Li radius.
[e]Taken from ^{7}Be radius.
[f]Taken from ^{8}B radius.

The two-body Shrödinger equation for a spherically-symmetric system is

$$\left(-\frac{\hbar^2}{2\mu}\nabla^2 + V(r) - E\right)\psi(r) = 0, \qquad (11)$$

where $\hbar$ is Planck's constant, μ is the reduced mass, $V(r)$ is the central potential at r, E is the energy, and $\psi(r)$ is the wave function at r. If the mass of the X^0 particle, i.e., m_X, is much heavier than the light nuclides, μ is approximately given by the mass of the nuclide.

The adopted RMS nuclear matter radii and their references are listed in columns 2 and 3 in Table I. Binding energies of ground state X nuclei are calculated with the interaction strength δ ($\delta_{\rm w}$) and the mass m_X taken as parameters. The obtained binding energies are used for the estimation of Q values of various reactions as described below. Similarly, we calculate binding energies of nuclear excited states of ${}^4{\rm He}_X^*$ and ${}^8{\rm Be}_X^*$ with relative angular momentum of $L = 1$ by solving Eq. (11) for the $L = 1$ states.

Figure 1 shows the contours of binding energies of ground state X nuclei from mass number $A = 1$ to 9 in the case of the Gaussian type XN potential. The contours correspond to binding energy (BE) of BE = 0.1 MeV. This value of energy is chosen since weakly bound X nuclei of BE $\lesssim O(0.1$ MeV) tend to be photodisintegrated by background radiations during BBN epoch. Such weakly bound nuclei can not attain their large abundances without suffering from destruction processes. In a parameter region located at right upper side from a contour, the X nucleus can form during BBN epoch, and thus possibly affects BBN.

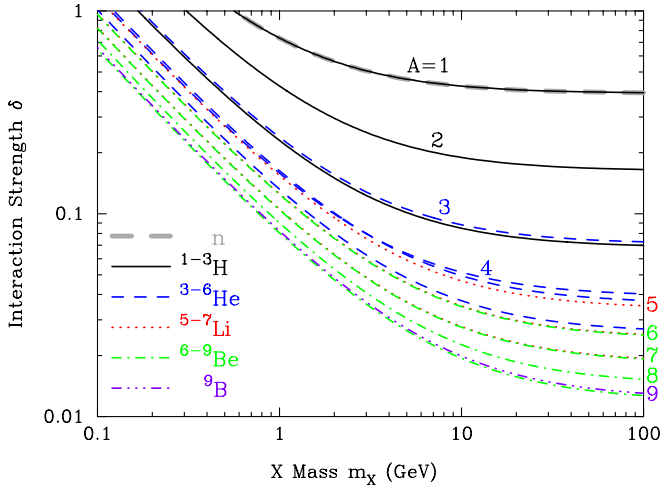

FIG. 1 (color online). Contours of binding energies between nuclei and an X^0 corresponding to 0.1 MeV for the case of the Gaussian XN potential. Numbers attached to the contours indicate mass numbers of nuclei.

Figure 2 shows similar contours of binding energies of BE = 0.1 MeV in the case of the well type XN potential. The shapes of contours in both potential cases are very similar and change slightly.

We adopt the Gaussian XN potential in calculating reaction rates and performing a network calculation of

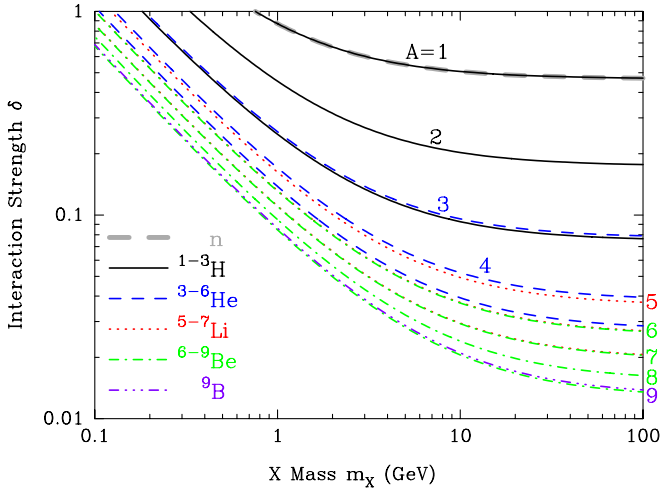

FIG. 2 (color online). Contours of binding energies between nuclei and an X^0 corresponding to 0.1 MeV for the case of the square well XN potential. Numbers attached to the contours indicate mass numbers of nuclei.

X-catalyzed BBN. After we introduce a mechanism of ^{7}Be destruction (this section) and show a result of the nucleosynthesis for the Gaussian XN potential (Secs. III A and III B), we delineate parameter regions for the ^{7}Be destruction of not only the Gaussian but also the well XN potentials in Sec. III C.

B. Reaction rates

Thermonuclear reaction rates $\langle\sigma v\rangle$ are roughly written (e.g., [102,103]) as

$$\langle\sigma v\rangle = \frac{(8/\pi)^{1/2}}{\mu^{1/2}(k_B T)^{3/2}} \int_0^\infty E\sigma(E)\exp(-E/k_B T)dE, \quad (12)$$

where σ is the cross section, v is the relative velocity, μ is the reduced mass of the system, k_B is the Boltzmann constant, T is the temperature, and E is the kinetic energy in the center of mass system. Since there is a relation, i.e., $E = \mu v^2/2$, the equation is identical to

$$\langle\sigma v\rangle = \frac{2/\pi^{1/2}}{(k_B T)^{3/2}} \int_0^\infty \sigma(E) v \exp(-E/k_B T)E^{1/2}dE. \quad (13)$$

Reactions of a neutral particle and charged nuclei occur without the effect of Coulomb repulsion. If the quantity, i.e., $\sigma(E)v$, is approximately given by $a + bE$ as a linear function of E, then the reaction rate is simply given by

$$N_A\langle\sigma v\rangle = N_A\left(a + \frac{3}{2}bk_B T\right), \quad (14)$$

where the Avogadro's number $N_A = 6.022 \times 10^{23}$ was multiplied to both sides of the equation. When the product, $\sigma(E)v$, does not change drastically around some fixed point of E, the integral in Eq. (13) receives a contribution from an energy region below $E \sim k_B T$. Information from cross sections in higher energies is, therefore, not involved in the integral.

Reactions triggered by two charged particles are, on the other hand, affected by the Coulomb force. The astrophysical S factor is defined as

$$S(E) = \sigma(E)E\exp\left(\frac{2\pi Z_1 Z_2 e^2}{\hbar v}\right), \quad (15)$$

where Z_1 and Z_2 are the charge numbers of interacting particles. The S factor might be well described by a linear function of E, i.e., $S(E) = S(E_0) + \alpha(E - E_0) = S(0) + \alpha E$, where $E_0 = 0.122(Z_1 Z_2)^{2/3}A^{1/3}T_9^{2/3}$ MeV is the most effective energy in the integral in Eq. (12). We defined $A \equiv \mu/(1\ \text{amu})$ and $T_9 \equiv T/(10^9\ \text{K})$. The reaction rate can then be written [15] in the form of

$$N_A\langle\sigma v\rangle = 7.82 \times 10^6\left(\frac{Z_1 Z_2}{\mu}\right)^{1/3} \times \left(\frac{S(0)}{\text{keVb}}\right)T_9^{-2/3}\exp\left[-\frac{4.25(Z_1^2 Z_2^2 A)^{1/3}}{T_9^{1/3}}\right] \times \left\{1 + \frac{(\alpha/\text{b})}{[S(0)/(\text{keVb})]}[122(Z_1^2 Z_2^2 A)^{1/3}T_9^{2/3} + 71.8T_9]\right\}\ \text{cm}^3\,\text{s}^{-1}\,\text{mol}^{-1}, \quad (16)$$

where the Avogadro's number N_A was multiplied, and $1\text{b} = 10^{-24}\ \text{cm}^2$ was used.

We estimate rates of several important reactions in this study. For both reactions by a neutral plus a charged particle and those by two charged particles, calculated rates are used to derive linear fitting functions to be adopted at the energy range relevant to BBN, i.e., $T_9 \lesssim 1$.

We here assume that the mass of the X^0 particle, i.e., m_X is 100 GeV. Calculations of nucleosynthesis are performed assuming the Gaussian XN nuclear potential as set up in Sec. II A. We show results of the BBN catalyzed by the X^0 particle for two cases of different strengths of XN interaction, i.e., $\delta = 0.1$ (Case 1) and 0.2 (Case 2) in what follows.

In this scenario of BBN catalyzed by the X^0 particle, the ^{7}Be can be destroyed at its X capture (Sec. II B 1). The efficiency of this destruction, however, depends upon the fraction of the X^0 particle escaping from the capture by ^{4}He (Sec. II B 2). Since other reactions of X nuclei can lead to productions of heavy nuclei, rates for such reactions are also estimated. Using reaction rates estimated as described in Secs. II B 1–II B 4 in our nuclear reaction network (Sec. II B 5), we perform a calculation of the catalyzed BBN.

The adopted reaction rates $N_A\langle\sigma v\rangle$, per second per (mole cm^{-3}), are shown in Tables II and III. Reaction Q values are derived taking account of the calculated binding energies of the X nuclei for Cases 1 and 2 (columns 4 and 5 in Table I). We use the notation, i.e., 1(2,3)4 for a reaction $1 + 2 \rightarrow 3 + 4$. Reaction rates related with the X^0 particle are estimated as follows.

1. Nonradiative reactions

$X(^7\text{Be}, ^3\text{He})^4\text{He}_X$.—This reaction is most important in this scenario. Its reaction rate is rather large since no radiation is involved in the reaction. It operates through the nonresonant process unless there are resonant states lying near the energy level of initial scattering state. We then adopt the nonresonant component of rate [105] for the normal nuclear reaction, i.e., $^6\text{Li}(n, \alpha)^3\text{H}$ as a rough approximation. The nonresonant component of the rate for this reaction can be extracted most easily of all (n, α) reactions on light nuclides. This is because heavy nuclides have large densities of resonance so that they tend to have many resonant components for nuclear reactions [106].

TABLE II. Reaction rates for $(m_X, \delta) = (100\ \mathrm{GeV}, 0.1)$.

Reaction	Reaction rate ($\mathrm{cm^3\ s^{-1}\ mole^{-1}}$)	Energy (MeV)[a]	Reverse coefficient[b]	Q_9[c]
$X(^6\mathrm{Li}, d)^4\mathrm{He}_X$	3.8×10^6	...	4.919	14.556
$^6\mathrm{Li}_X(p, ^3\mathrm{He}\alpha)X$	$3.6 \times 10^{10} T_9^{-2/3} \exp(-8.81/T_9^{1/3})$	...	...	35.421
$^6\mathrm{Be}_X(, e^+\nu_e)^6\mathrm{Li}_X$	$1.9\ (\mathrm{s^{-1}})$	...	...	44.225
$X(^4\mathrm{He}, \gamma)^4\mathrm{He}_X$	$2.3 \times 10^2 + 2.6 \times 10^3 T_9$	...	7.472	31.659
$^4\mathrm{He}_X(d, \gamma)^6\mathrm{Li}_X$	$1.0 \times 10^4 T_9^{-2/3} \exp(-8.45/T_9^{1/3})(1 + 6.9T_9^{2/3} + 2.0T_9)$	0.15–0.25	2.717	28.331
$X(^7\mathrm{Li}, t)^4\mathrm{He}_X$	2.9×10^6	...	6.748	3.034
$X(^7\mathrm{Be}, ^3\mathrm{He})^4\mathrm{He}_X$	2.9×10^6	...	6.748	13.252
$^4\mathrm{He}_X(\alpha, \gamma)^8\mathrm{Be}_X$	$7.8 \times 10^5 T_9^{-2/3} \exp(-16.79/T_9^{1/3})(1 - 0.39T_9^{2/3} - 0.058T_9)$	0–1	7.487	45.509
	$+4.8 \times 10^5 T_9^{-2/3} \exp(-16.79/T_9^{1/3})(-1 + 2.1T_9^{2/3} + 0.32T_9)$	0.3–0.5		
$^8\mathrm{Be}_X(d, p)^9\mathrm{Be}_X$	$9.8 \times 10^{11} T_9^{-2/3} \exp(-13.49/T_9^{1/3})$[d]	...	1.060	7.242

[a]Rates are estimated by linear fits of S factors in the energy ranges.
[b]For nuclides $a = i, j, k, \ldots$ with mass numbers A_a and numbers of magnetic substates g_a, the reverse coefficients are defined as in Ref. [104]: $0.9867(g_i g_j/g_k)(A_{i_X} A_j/A_{k_X})^{3/2}$ for the process $i_X(j,\gamma)k_X$, and $[g_i g_j/(g_k g_l)][A_{i_X} A_j/(A_k A_{l_X})]^{3/2}$ for the process $i_X(j,k)l_X$.
[c]$Q_9 \equiv 11.605\ (Q/\mathrm{MeV})$.
[d]The rate in Ref. [4] is taken.

The dependence of cross section on the reduced mass μ (or A in atomic mass units), i.e., $\sigma \propto A^{-2}$ has been used to correct for de Broglie wavelengths.

Other X-capture reactions.—Similarly, reaction rates of $X(^6\mathrm{Li}, d)^4\mathrm{He}_X$, $X(^7\mathrm{Li}, t)^4\mathrm{He}_X$, $X(^7\mathrm{Be}, p)^6\mathrm{Li}_X$ and $X(^7\mathrm{Be}, n)^6\mathrm{Be}_X$ [107] are also taken from that of $^6\mathrm{Li}(n, \alpha)^3\mathrm{H}$. They are corrected for the reduced masses.

In Case 1, the Q values of $X(^7\mathrm{Be}, p)^6\mathrm{Li}_X$ and $X(^7\mathrm{Be}, n)^6\mathrm{Be}_X$ are negative. The reactions are then neglected as well as their inverse reactions which would never become important in changing the abundance of ^{7}Be due to small abundances of $^6\mathrm{Li}_X$ and $^6\mathrm{Be}_X$ as shown in Section III A.

Destruction of $^6\mathrm{Li}_X$.—The main proton burning reaction of $^6\mathrm{Li}_X$ is $^6\mathrm{Li}_X(p, ^3\mathrm{He})^4\mathrm{He}_X$ in Case 2. In Case 1, on the other hand, the Q value of a three-body breakup reaction $^6\mathrm{Li}_X(p, ^3\mathrm{He}\alpha)X$ is positive. Its cross section is then much larger than that of $^6\mathrm{Li}_X(p, ^3\mathrm{He})^4\mathrm{He}_X$ due to a larger phase space in the final state. This situation is the same as that in a similar reaction catalyzed by a long-lived negatively charged particle X^- [15]. The reaction rates of $^6\mathrm{Li}_X(p, ^3\mathrm{He}\alpha)X$ (Case 1) and $^6\mathrm{Li}_X(p, ^3\mathrm{He})^4\mathrm{He}_X$ (Case 2)

TABLE III. Reaction rates for $(m_X, \delta) = (100\ \mathrm{GeV}, 0.2)$.

Reaction	Reaction rate ($\mathrm{cm^3\ s^{-1}\ mole^{-1}}$)	Energy (MeV)[a]	Reverse coefficient[b]	Q_9[c]
$X(^6\mathrm{Li}, d)^4\mathrm{He}_X$	3.8×10^6	...	4.919	96.708
$X(^7\mathrm{Be}, n)^6\mathrm{Be}_X$	2.9×10^6	...	34.139	0.130
$X(^7\mathrm{Be}, p)^6\mathrm{Li}_X$	2.9×10^6	...	11.380	56.727
$^6\mathrm{Li}_X(p, ^3\mathrm{He})^4\mathrm{He}_X$	$3.6 \times 10^{10} T_9^{-2/3} \exp(-8.81/T_9^{1/3})$	...	0.593	38.678
$^6\mathrm{Be}_X(, e^+\nu_e)^6\mathrm{Li}_X$	$6.2 \times 10^{-10}\ (\mathrm{s^{-1}})$	...	...	44.225
$X(^4\mathrm{He}, \gamma)^4\mathrm{He}_X$	$5.0 \times 10^4 - 2.2 \times 10^3 T_9$	...	7.472	113.811
$^4\mathrm{He}_X(d, \gamma)^6\mathrm{Li}_X$	$8.2 \times 10^3 T_9^{-2/3} \exp(-8.45/T_9^{1/3})(-1 + 6.6T_9^{2/3} + 2.0T_9)$	0.15–0.25	2.717	25.074
$X(^7\mathrm{Li}, t)^4\mathrm{He}_X$	2.9×10^6	...	6.748	85.186
$X(^7\mathrm{Be}, ^3\mathrm{He})^4\mathrm{He}_X$	2.9×10^6	...	6.748	95.404
$^4\mathrm{He}_X(\alpha, \gamma)^8\mathrm{Be}_X$	$2.4 \times 10^4 T_9^{-2/3} \exp(-16.79/T_9^{1/3})(1 + 0.15T_9^{2/3} + 0.022T_9)$	0–1	7.487	82.366
	$+2.7 \times 10^4 T_9^{-2/3} \exp(-16.79/T_9^{1/3})(-1 + 2.7T_9^{2/3} + 0.41T_9)$	0.3–0.5		
$^8\mathrm{Be}_X(d, p)^9\mathrm{Be}_X$	$9.8 \times 10^{11} T_9^{-2/3} \exp(-13.49/T_9^{1/3})$[d]	...	1.060	20.957

[a]Rates are estimated by linear fits of S factors in the energy ranges.
[b]For nuclides $a = i, j, k, \ldots$ with mass numbers A_a and numbers of magnetic substates g_a, the reverse coefficients are defined as in Ref. [104]: $0.9867(g_i g_j/g_k)(A_{i_X} A_j/A_{k_X})^{3/2}$ for the process $i_X(j,\gamma)k_X$, and $[g_i g_j/(g_k g_l)][A_{i_X} A_j/(A_k A_{l_X})]^{3/2}$ for the process $i_X(j,k)l_X$.
[c]$Q_9 \equiv 11.605\ (Q/\mathrm{MeV})$.
[d]The rate in Ref. [4] is taken.

were both taken from that of $^6\mathrm{Li}(p, \alpha)^3\mathrm{He}$. In the expression for a nonresonant contribution to the thermonuclear reaction rate [Eq. (16)], the reduced mass was corrected. The survival of $^6\mathrm{Li}_X$ thus differs from that of ^{6}Li due to only the change in reduced masses of initial states relative to $^6\mathrm{Li}(p, \alpha)^3\mathrm{He}$.

Production of $^9\mathrm{Be}_X$.—Since the reaction $^4\mathrm{He}_X(\alpha, \gamma)^8\mathrm{Be}_X$ is found to be responsible for an accumulation of $^8\mathrm{Be}_X$ both in Cases 1 and 2 (see Sec. III), flows of nuclear abundances toward higher mass numbers should be calculated. The most important reactions in this regard are $^8\mathrm{Be}_X(d, p)^9\mathrm{Be}_X$ and $^8\mathrm{Be}_X(d, n)^9\mathrm{B}_X$ [4]. The reaction rates of $^8\mathrm{Be}_X(d, p)^9\mathrm{Be}_X$ are taken from that of $^7\mathrm{Be}_X(d, p\alpha)^4\mathrm{He}_X$ corrected for the reduced mass [4]. The Q values of $^8\mathrm{Be}_X(d, n)^9\mathrm{B}_X$ are negative. This reaction can, therefore, be neglected in environments of relatively low temperatures such as BBN.

2. Radiative nuclear reactions

We estimate rates of radiative capture reactions which can be important to leave signatures of the X^0 particle on primordial abundances of light elements. Wave functions of bound and continuum states are derived with the code RADCAP published by Bertulani [108], which was modified and given proper input parameters described below. The code also calculates cross sections of forward and reverse reactions, and astrophysical S factors.

$X(\alpha, \gamma)^4\mathrm{He}_X$.—This reaction is very important for the existence of parameter region in which the primordial ^{7}Li abundance is reduced. The abundance of the free X^0 decreases if the strongly-interacting X^0 particle is quickly captured by ^{4}He after ^{4}He nuclei are produced abundantly in the BBN epoch. Heavy nuclei such as ^{6,7}Li and ^{7}Be whose abundances build up after the ^{4}He production are then not affected by free X^0 particles. The $^4\mathrm{He}_X$ nuclei can not react efficiently with Li and Be nuclei due to large Coulomb repulsion forces by them.

Note also that the reaction between ^{4}He and X^0 is mainly through a radiative capture. The critical binding energies of ^{3}H and ^{3}He to an X^0 at which Q values of $X(\alpha, N)^3A_X$ reactions change from negative to positive are very high (see Table IV). These high binding energies are not realized in the cases of relatively weak XN interaction considered in this investigation.

Whether a given reaction operates efficiently enough to change an abundance of relevant particle species is roughly determined by a comparison of its rate Γ and the cosmic expansion rate H. For a reduction of the X^0 abundance via a radiative capture by ^{4}He, the Γ/H ratio is given by

$$\frac{\Gamma}{H} = \left(\frac{Y}{0.25}\right)\left(\frac{\eta}{6.2\times10^{-10}}\right)\left(\frac{T}{0.1\ \mathrm{MeV}}\right) \times\left(\frac{N_A\langle\sigma v\rangle}{1.9\times10^3\ \mathrm{cm^3\ s^{-1}\ mol^{-1}}}\right), \quad (17)$$

TABLE IV. Critical binding energies of X-nuclei.

Number	Reaction	Binding energy (MeV)
1	$X(^2\mathrm{H}, n)^1\mathrm{H}_X$	2.224
2	$X(^2\mathrm{H}, p)^1n_X$	2.224
3	$X(^3\mathrm{H}, n)^2\mathrm{H}_X$	6.257
4	$X(^3\mathrm{He}, p)^2\mathrm{H}_X$	5.494
5	$X(^4\mathrm{He}, p)^3\mathrm{H}_X$	19.815
6	$X(^4\mathrm{He}, n)^3\mathrm{He}_X$	20.578
7	$X(^6\mathrm{Li}, p)^5\mathrm{He}_X$	4.497
8	$X(^6\mathrm{Li}, n)^5\mathrm{Li}_X$	5.39
9	$X(^7\mathrm{Li}, p)^6\mathrm{He}_X$	9.975
10	$X(^7\mathrm{Li}, n)^6\mathrm{Li}_X$	7.250
11	$X(^7\mathrm{Be}, p)^6\mathrm{Li}_X$	5.606
12	$X(^7\mathrm{Be}, n)^6\mathrm{Be}_X$	10.676
13	$X(^4\mathrm{He}, d)^2\mathrm{H}_X$	23.848
14	$X(^6\mathrm{Li}, d)^4\mathrm{He}_X$	1.474
15	$X(^7\mathrm{Li}, t)^4\mathrm{He}_X$	2.467
16	$X(^7\mathrm{Be}, ^3\mathrm{He})^4\mathrm{He}_X$	1.587

where Y is the ratio by mass of ^{4}He to total baryon, and η is the baryon-to-photon ratio. If $\Gamma/H > 1$, then the reaction $X(\alpha, \gamma)^4\mathrm{He}_X$ quickly decreases the abundance of the free X^0 particle.

In Case 1, the ground state of $^4\mathrm{He}_X$ exists although excited states do not. Because of the selection rule for electromagnetic multipole transitions, an electric dipole (E1) transition from a relative s-wave scattering state into the ground s-wave bound state is not allowed. The cross section then has a predominant contribution from an E1 transition from a p-wave scattering state.

In Case 2, there is one excited state of $^4\mathrm{He}_X$ with relative angular momentum of $L = 1$ (see Table I). The selection rule then allows an E1 transition from a relative s-wave scattering state into the excited p-wave bound state.

For both cases the nuclear potential is given by Eq. (10) in calculating wave functions of the ground and excited states and scattering states of the ^{4}He and X^0 system with the code RADCAP. Adopting $r_{\mathrm{m}}^{\mathrm{RMS}} = 1.59$ fm, i.e., $b = 1.30$ fm, the potential is given numerically by

$$V_{\mathrm{N}}(r) = -123\ \mathrm{MeV}\,\delta\exp\{-[r/(1.97\ \mathrm{fm})]^2\}. \quad (18)$$

$^4\mathrm{He}_X(d, \gamma)^6\mathrm{Li}_X$.—We calculate the radiative capture cross section with the two-body model for the system of a $^4\mathrm{He}_X$ and a deuteron. The cross section is proportional to the electromagnetic matrix element squared [108]. The matrix element is an integral over space of the scattering and bound state wave functions and the operator. The E1 operator is estimated from the initial state wave function. The operator is $e_1 r Y_{1\mu}(\hat{r})$ for the radius $\boldsymbol{r}$ from the center of mass with the effective charge $e_1 = e(m_{^4\mathrm{He}_X} - 2_{m_d})/(m_{^4\mathrm{He}_X} + m_d)$, and $e_1 \to e$ in the limit of an infinitely massive X^0 particle. Although the wave function of the $^4\mathrm{He}_X - d$ system should be used in calculating the matrix

element, as one method we approximately take the wave function of the $^6\mathrm{Li}-X$ bound state calculated with Eq. (19) as that of the $^4\mathrm{He}_X - d$ bound state. As described hereinbelow, we try another method in which the wave function of the $^6\mathrm{Li}_X$ nucleus is calculated by the two-body model for the $^4\mathrm{He}_X - d$ system with its interaction tuned to reproduce binding energies of $^6\mathrm{Li}_X$. Three-body (^{4}He, d, and X^0) quantum mechanical calculations are necessary for more consistent estimations of cross sections without the approximation.

The nuclear potential for the ground state of $^6\mathrm{Li}_X$ in the final state is given by Eq. (10) in calculating the bound state wave function only. Adopting $r_{\mathrm{m}}^{\mathrm{RMS}} = 2.35$ fm, i.e., $b = 1.92$ fm, the potential is given numerically by

$$V_{\mathrm{N}}(r) = -99.2\ \mathrm{MeV}\delta \exp\{-[r/(2.43\ \mathrm{fm})]^2\}. \quad (19)$$

The nuclear potential for initial scattering states of $^4\mathrm{He}_X$ and d was taken from that between X^0 and d and that between ^{4}He which is bound to the X^0 and d. The former is given by Eq. (10). Adopting $r_{\mathrm{m}}^{\mathrm{RMS}} = 1.97$ fm, i.e., $b = 1.61$ fm, the potential is given numerically by

$$V_{\mathrm{N}}^{X-d}(r) = -45.0\ \mathrm{MeV}\delta \exp\{-[r/(2.19\ \mathrm{fm})]^2\}. \quad (20)$$

The latter is given by

$$V(r)_{\mathrm{N}}^{\alpha(\mathrm{B})-d} = \int \rho(\boldsymbol{r}')V_{\mathrm{N}}^{\alpha-d}(\boldsymbol{x})d\boldsymbol{r}' = \frac{2\pi}{r}\int_0^\infty dr' r'\rho(r')\int_{|r-r'|}^{r+r'} dx x V_{\mathrm{N}}^{\alpha-d}(x), \quad (21)$$

where $\boldsymbol{r}$ is the radius from the center of mass of $^4\mathrm{He}_X$ to that of d, $\boldsymbol{r}'$ is the distance between the position of $^4\mathrm{He}_X$ to that of the ^{4}He nucleus, $\boldsymbol{x} = \boldsymbol{r} + \boldsymbol{r}'$ is the distance between the deuteron and ^{4}He, and $\rho(\boldsymbol{r}')$ is the distribution function of ^{4}He, $V_{\mathrm{N}}^{\alpha-d}(x)$ is the nuclear potential between a free α particle and a deuteron, and spherical symmetries in $\rho(\boldsymbol{r}')$ and $V_{\mathrm{N}}^{\alpha-d}(\boldsymbol{x})$ were assumed in the last equality.

The potential $V_{\mathrm{N}}^{\alpha-d}$ is given by the two-component Gaussian function

$$V_{\mathrm{N}}^{\alpha-d}(r) = \sum_{i=1}^{2} V_i \exp[-(r/r_i)^2], \quad (22)$$

where $V_1 = 500$ MeV, $r_1 = 0.9$ fm, $V_2 = -64.06$ MeV, and $r_2 = 2.0$ fm [15]. The potential $V(r)_{\mathrm{N}}^{\alpha(\mathrm{B})-d}$ is then rewritten in the form of

$$V(r)_{\mathrm{N}}^{\alpha(\mathrm{B})-d} = \frac{\pi}{r}\sum_i V_i r_i^2 \int_0^\infty dr' r'\rho(r') \times \left\{\exp\left[-\left(\frac{r-r'}{r_i}\right)^2\right] - \exp\left[-\left(\frac{r+r'}{r_i}\right)^2\right]\right\}. \quad (23)$$

The Coulomb potentials for initial scattering states of $^4\mathrm{He}_X$ and d originate only from that between ^{4}He (inside $^4\mathrm{He}_X$) and d. It is approximately given [15] by

$$V_{\mathrm{C}}^{\alpha(\mathrm{B})-d}(r) = Z_{^4\mathrm{He}_X} Z_d e^2 \frac{\mathrm{erf}\left(r/\sqrt{b_{^4\mathrm{He}_X}^2 + b_d^2}\right)}{r}, \quad (24)$$

where $Z_{^4\mathrm{He}_X} = 2$ is the electric charge of $^4\mathrm{He}_X$ nucleus, $b_{^4\mathrm{He}_X}$ and b_d are ranges for charges of $^4\mathrm{He}_X$ and deuteron, respectively. $b_d = 1.47$ fm is assumed, which is derived from $b_d = \sqrt{2/3}r_{\mathrm{C}}^{\mathrm{RMS}}$ and the RMS charge radius value of $r_{\mathrm{C}}^{\mathrm{RMS}} = 1.4696$ fm [109]. We take as the $b_{^4\mathrm{He}_X}$ value the radius at which the charge density $\rho_{\mathrm{C}}(r)$ of $^4\mathrm{He}_X$ is $\exp(-2)$ times the maximum value, i.e, $\rho_{\mathrm{C}}(0)$.

The charge density of A_X is given by

$$\rho_{\mathrm{C},A_X}(r) = \int \rho_{A_X}(\boldsymbol{r}')\rho_{\mathrm{C},A}(\boldsymbol{r}'')d\boldsymbol{r}' = \frac{2Ze}{\sqrt{\pi}br}\int_0^\infty dr' r'\rho_{A_X}(r') \times \left\{\exp\left[-\left(\frac{r-r'}{b}\right)^2\right] - \exp\left[-\left(\frac{r+r'}{b}\right)^2\right]\right\}, \quad (25)$$

where $\boldsymbol{r}'$ is the radius from the center of mass of A_X to that of A, $\boldsymbol{r}''$ is the position vector of charge contributed by the nucleus, $r = |\boldsymbol{r}' + \boldsymbol{r}''|$ is the distance from the center of mass of A_X, $\rho_{A_X}(\boldsymbol{r}')$ is the distribution function of A, and $\rho_{\mathrm{C},A}(\boldsymbol{r}'')$ is the charge density of the nucleus. The nuclear charge density was assumed to be $\rho_{\mathrm{C},A}(\boldsymbol{r}'') = Ze(\pi b^2)^{-3/2}\exp[-(r''/b)^2]$ in the last equality. The range parameter, i.e., b for ^{4}He is given by $b_{^4\mathrm{He}} = \sqrt{2/3}r_{\mathrm{C}}^{\mathrm{RMS}}$ and the RMS charge radius value of $r_{\mathrm{C}}^{\mathrm{RMS}} = 1.80$ fm [100].

The charge densities of $^4\mathrm{He}_X$ are calculated, and the ranges of charge distribution are derived: $b_{^4\mathrm{He}_X} = 2.97$ fm ($\delta = 0.1$) and 2.64 fm ($\delta = 0.2$). They are used in Eq. (24).

Figure 3 shows the adopted nuclear potential V_{N}^{X-d} and the calculated distribution function, i.e., ρ, and charge density, i.e., ρ_{C}, of $^4\mathrm{He}_X$, and nuclear ($V_{\mathrm{N}}^{\alpha(\mathrm{B})-d}$) and Coulomb ($V_{\mathrm{C}}^{\alpha(\mathrm{B})-d}$) potentials (solid lines) for Case 1 ($\delta = 0.1$) as a function of radius from the center of mass of $^4\mathrm{He}_X$. The center of mass is approximated to be the position of X^0 since the mass of X^0 is much larger than that of nucleon.

Figure 4 shows similar potentials and densities (solid lines) for Case 2 ($\delta = 0.2$).

We calculate rates using another method for the same reaction. We assume that the $^6\mathrm{Li}_X$ nucleus in the final state is described as the two-body bound state of the $^4\mathrm{He}_X - d$ system. Both of initial and final state wave functions are generated from a $^4\mathrm{He} - d$ potential tuned to reproduce the binding energy of $^6\mathrm{Li}_X$ relative to separated $^4\mathrm{He}_X$ and deuteron consistent with results in Table I [2.44 MeV for Case 1 ($\delta = 0.1$) and 2.16 MeV for Case 2 ($\delta = 0.2$)]. We use potential terms given by Eqs. (20), (23), and (24). The parameter δ in the nuclear potential between an X^0 and a

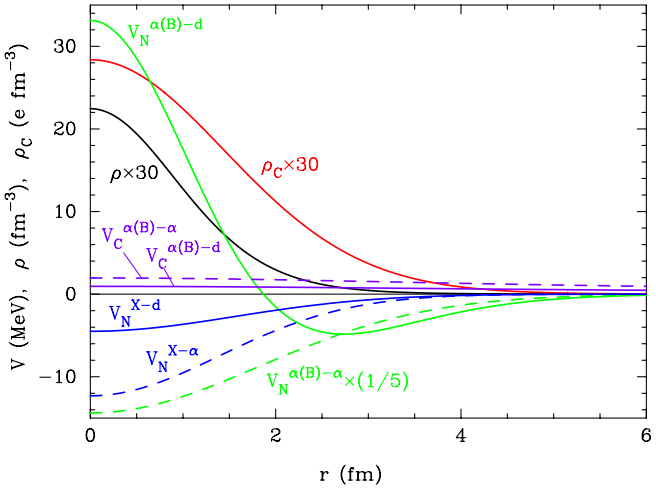

FIG. 3 (color online). Nuclear potentials between an α and a deuteron ($V_{\rm N}^{\alpha({\rm B})-d}$), an X^0 and a deuteron ($V_{\rm N}^{X-d}$), and the Coulomb potential between an α and a deuteron ($V_{\rm C}^{\alpha({\rm B})-d}$) as a function of distance from the center of mass of the $^4{\rm He}_X + d$ system (solid lines). The similar potentials for the $^4{\rm He}_X + \alpha$ system (dashed lines), the distribution function (ρ), and the charge density ($\rho_{\rm C}$) of $^4{\rm He}_X$ (solid lines) are also drawn. It was assumed that the mass of X^0 particle is $m_X = 100$ GeV and that the interaction strength of XN force is 0.1 times that of NN force ($\delta = 0.1$).

deuteron [Eq. (20)] is fitted: $\delta_{\rm fit} = 0.494$ for Case 1 and $\delta_{\rm fit} = 0.373$ for Case 2. Calculated reaction rates are as follows:

$$N_A\langle\sigma v\rangle = 1.9 \times 10^4 T_9^{-2/3} \exp(-8.45/T_9^{1/3})(1 + 2.6T_9^{2/3} + 0.78T_9)\ {\rm cm}^3{\rm s}^{-1}\,{\rm mol}^{-1} \quad (26)$$

for Case 1 ($\delta = 0.1$), and

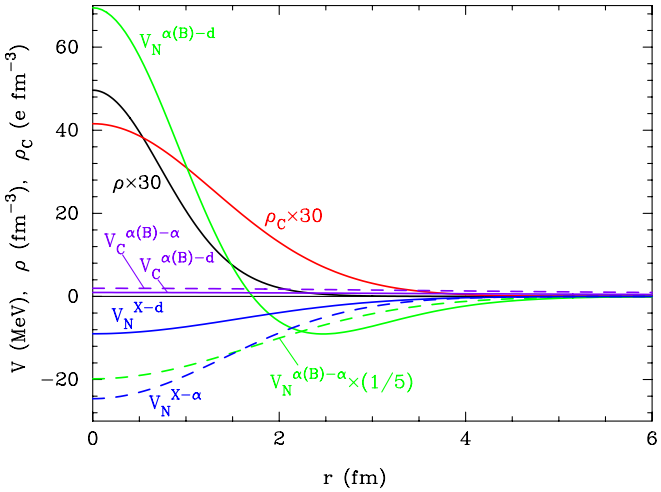

FIG. 4 (color online). Same as in Fig. 3 when the interaction strength of XN force is 0.2 times that of NN force ($\delta = 0.2$).

$$N_A\langle\sigma v\rangle = 1.7 \times 10^4 T_9^{-2/3} \exp(-8.45/T_9^{1/3})(1 + 3.6T_9^{2/3} + 1.1T_9)\ {\rm cm}^3{\rm s}^{-1}\,{\rm mol}^{-1} \quad (27)$$

for Case 2 ($\delta = 0.2$). These rates differ from our standard rates in Tables II and III by 17–26% (Case 1) and −45– − 33% (Case 2), respectively, in the important temperature range of $T_9 = 0.5$–1 corresponding to $E_0 = 0.15$–0.25 MeV.

$^4{\rm He}_X(\alpha, \gamma)^8{\rm Be}_X$.—In both of Cases 1 and 2, there is one excited state of $^8{\rm Be}_X$ with $L = 1$ below the energy level of the initial separation channel of $^4{\rm He}_X$ and α. The excitation energies are 3.72 MeV ($\delta = 0.1$) and 5.89 MeV ($\delta = 0.2$), respectively. Both rates for final states of the $^8{\rm Be}_X$ ground and excited states are then calculated.

The nuclear potential for the ground state of $^8{\rm Be}_X$ in the final state is given by Eq. (10) in calculating the wave function. Adopting $r_{\rm m}^{\rm RMS} = 2.33$ fm, i.e., $b = 1.90$ fm, the potential is given numerically by

$$V_{\rm N}(r) = -134\ {\rm MeV}\,\delta \exp\{-[r/(2.41\ {\rm fm})]^2\}. \quad (28)$$

We calculate cross sections by the two-body model in the same procedure as performed for the previous reaction, i.e., $^4{\rm He}_X(d, \gamma)^6{\rm Li}_X$. The nuclear potential between two free α particles was taken from the three-component Gaussian function

$$V_{\rm N}^{\alpha-\alpha}(r) = \sum_{i=1}^{3} V_i \exp[-(r/r_i)^2], \quad (29)$$

where $V_1 = -1.742$ MeV, $r_1 = 3.00$ fm, $V_2 = -395.9$ MeV, $r_2 = 1.90$ fm, $V_3 = 299.4$ MeV, and $r_3 = 1.74$ fm [96].

The adopted nuclear potential $V_{\rm N}^{X-\alpha}$ and the calculated nuclear ($V_{\rm N}^{\alpha({\rm B})-\alpha}$) and Coulomb ($V_{\rm C}^{\alpha({\rm B})-\alpha}$) potentials (dashed lines) for Case 1 ($\delta = 0.1$) are shown as a function of radius from the center of mass of $^4{\rm He}_X$ in Fig. 3. Similar potentials (dashed lines) for Case 2 ($\delta = 0.2$) are shown in Fig. 4.

First and second terms of reaction rates in Tables II and III are calculated rates for transitions to the ground and excited states, respectively. The reaction leading to the ground state is via an E1 transition from an initial p-wave scattering state, while that leading to the excited state is predominantly an E1 transition from an initial s-wave scattering state.

3. β decay

The reaction rate of $^6{\rm Be}_X(, \beta^+\nu_e)^6{\rm Li}_X$ is estimated using that of ^{6}He(, $\beta^-\bar{\nu}_e)^6$Li. It was corrected for a phase space factor related to the reaction Q value. The rate is then given by $\Gamma_X = (\ln 2/T_{1/2})(Q_X/Q)^5$, where $T_{1/2}$ is the half life of ^{6}He, Q_X and Q are the Q values for the β decay of $^6{\rm Be}_X$ and ^{6}He, respectively. $T_{1/2} = (806.7 \pm 1.5)$ ms and

$Q = 3.508$ MeV are adopted [110]. See Tables II and III for derived Q_X values.

4. Unimportant pathways through $^5\mathrm{He}_X$ and $^5\mathrm{Li}_X$

Reactions of $^5\mathrm{He}_X$ and $^5\mathrm{Li}_X$ are found to be unimportant in this study under the assumption of our models described above.

The binding of the X^0 particle to ^{5}He and ^{5}Li can lead to stabilizations of such bound states against neutron and proton emissions, respectively [4]. This study, however, indicates that ^5A_X nuclei do not play a significant role in the BBN epoch in both Cases 1 and 2. The reason is as follows:

A sufficient condition for that the ^5A_X nuclei are not important for a production of heavy nuclei of $A > 6$ is satisfied in Cases 1 and 2: Q values of reactions $^4\mathrm{He}_X(d, n)^5\mathrm{Li}_X$ and $^4\mathrm{He}_X(d, p)^5\mathrm{He}_X$ are negative. This means that $^5\mathrm{Li}_X$ and $^5\mathrm{He}_X$ produced during BBN (if any via radiative captures of p or n by $^4\mathrm{He}_X$) is quickly processed by n or p back into $^4\mathrm{He}_X$ via $^5\mathrm{Li}_X(n, d)^4\mathrm{He}_X$ and $^5\mathrm{He}_X(p, d)^4\mathrm{He}_X$. Note that the destruction reactions are strong since no radiation is involved in the reactions.

In passing, if the energy level of $^5\mathrm{He}_X$ ($^5\mathrm{Li}_X$) nucleus is lower than that of $^4\mathrm{He}_X + n(p)$ separation channel, i.e., $Q(^4\mathrm{He}_X + N \rightarrow {}^5A_X) \gtrsim 0$ MeV, the X nucleus can be produced during BBN. Amounts of such X nuclei are, however, very small due to the reason explained in the previous paragraph. In this investigation, the ^5A_X nuclides have not been stabilized in both cases of potential types for parameter space studied. The ^5A_X nuclei then do not play a role. There is, however, a large uncertainty in binding energies of X nuclei which stems from XA potentials and from precise nucleon density of X nuclei. Such uncertain points should be studied using specific particle models describing potentials and dedicated quantum many-body models taking account of interactions inside the normal nuclei such as $^5A = {}^4\mathrm{He} + N$ during the processes.

5. Nuclear reaction network

We calculate binding energies of X nuclei and Q values of reactions involving the X^0 particle and X nuclei. We estimate rates of several (forward and reverse) reactions, which possibly play roles in BBN as described above, and calculated the catalyzed BBN. We note that productions of double X nuclei, i.e., A_{XX}, are not taken into account in this study. The ratio of the rate for reaction between X nuclei and an X^0 to that of cosmic expansion is given by

$$\frac{\Gamma}{H} = \left(\frac{n_X/n_b}{10^{-4}}\right)\left(\frac{\eta}{6.2\times10^{-10}}\right)\left(\frac{T}{0.1\ \mathrm{MeV}}\right) \times \left(\frac{N_A\langle\sigma v\rangle}{1.2\times10^{6}\ \mathrm{cm^3\,s^{-1}\,mol^{-1}}}\right). \quad (30)$$

An efficient operation of a reaction should satisfy $\Gamma/H > 1$, which is possible when $N_A\langle\sigma v\rangle \gtrsim 10^6\ \mathrm{cm^3\,s^{-1}\,mol^{-1}}$. X nuclei with significant abundances during the catalyzed BBN seen in Sec. III are $^4\mathrm{He}_X$, $^6\mathrm{Li}_X$, $^8\mathrm{Be}_X$ and $^9\mathrm{Be}_X$. $^4\mathrm{He}_X$ can react with an X^0 particle only via the radiative capture since there is no exit channel of particle break up. Since reaction rates of radiative capture are typically small, $^4\mathrm{He}_{XX}$ production is not efficient. The effect of $^4\mathrm{He}_{XX}$ would thus be negligible although some fraction of $^4\mathrm{He}_X$ would react with an X^0 and form the $^4\mathrm{He}_{XX}$. Other X nuclei, i.e., $^6\mathrm{Li}_X$, $^8\mathrm{Be}_X$ and $^9\mathrm{Be}_X$ can, on the other hand, react nonradiatively with an X^0. Possible reactions are $^6\mathrm{Li}_X(X, d)^4\mathrm{He}_{XX}$, $^8\mathrm{Be}_X(X, \alpha)^4\mathrm{He}_{XX}$, $^8\mathrm{Be}_X(X, \alpha_X)^4\mathrm{He}_X$, $^9\mathrm{Be}_X(X, n)^8\mathrm{Be}_{XX}$, and $^9\mathrm{Be}_X(X, \alpha n)^4\mathrm{He}_{XX}$ (whether their Q values are positive or negative should be determined by more sophisticated estimations of binding energies). Since abundances of $^6\mathrm{Li}_X$, $^8\mathrm{Be}_X$ and $^9\mathrm{Be}_X$ are rather small in cases studied in this paper (Sec. III), their processing would have negligible effects on final abundances of light elements. We note, however, that final abundances of $^6\mathrm{Li}_X$ and $^9\mathrm{Be}_X$ may be reduced through nonradiative reactions with an X^0 particle.

The BBN network code of Refs. [111,112] is modified and used. The X^0 particles and relevant X nuclei are included as new species. Reactions connecting normal and X nuclei and the X^0 particle are added to the code (see Tables II and III for their rates). Nuclear reaction rates for the SBBN [111,112] have been replaced with new rates published in Refs. [58,113], and the adopted neutron lifetime is $\tau_n = 881.9$ s [114].

III. RESULTS

A. Evolution of nuclear abundances

Figure 5 shows results of the abundances of normal and X nuclei as a function of temperature for Case 1 ($\delta = 0.1$). The mass of the X^0 has been taken to be $m_X = 100$ GeV. Its initial abundance is $N_X/n_b = 1.7\times10^{-4}$ ($Y_X \equiv N_X/s = 1.5\times10^{-14}$), where N_X and n_b are the number densities of the X^0 particles and baryons, respectively. This abundance is chosen as an example leading to a significant ^{7}Be reduction. It is set as a parameter here since the X^0 abundance is very uncertain. The decay lifetime is assumed to be much longer than BBN time scale, i.e., $\tau_X \gg 200$ s so that effects of the decay are not seen. The X^0 particle is assumed to have been long extinct by now.

At high temperatures $T_9 \gtrsim 1$, the X^0 particles exist mainly in the free state since efficient photodisintegrations of X nuclei destroy the bound state. At $T_9 \sim 1$, the ^{4}He synthesis occurs as in SBBN, and about one third of X^0 particles are then captured by ^{4}He nuclei. $^4\mathrm{He}_X$ nuclei produced in this epoch react with normal nuclei and affect abundances of ^{7}Li [by $^4\mathrm{He}_X(t, {}^7\mathrm{Li})X$ [115]], $^6\mathrm{Li}_X$ [by $^4\mathrm{He}_X(d, \gamma)^6\mathrm{Li}_X$], and $^8\mathrm{Be}_X$ [by $^4\mathrm{He}_X(\alpha, \gamma)^8\mathrm{Be}_X$]. Note that $^6\mathrm{Li}_X$ nuclei produced at $T_9 \sim 1$ experience a strong destruction process, i.e., $^6\mathrm{Li}_X(p, {}^3\mathrm{He}\alpha)X$. $^9\mathrm{Be}_X$ is produced by $^8\mathrm{Be}_X(d, p)^9\mathrm{Be}_X$. At last, the most important processes operate. Free X^0 particles which survived the

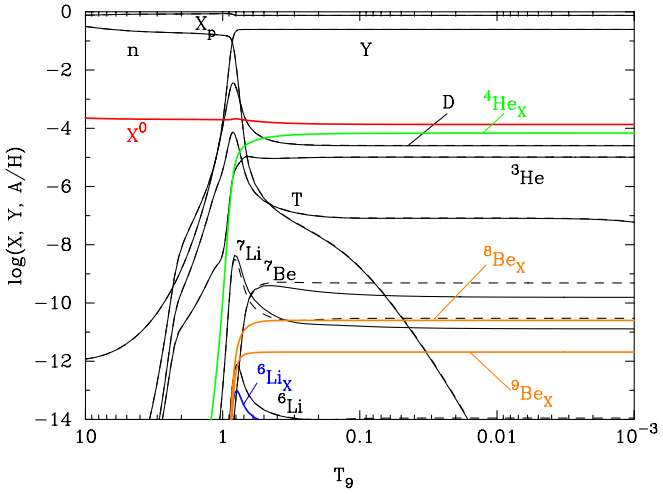

FIG. 5 (color online). Calculated abundances of normal and X nuclei (solid lines) as a function of T_9. The mass of X^0 particle was assumed to be $m_X = 100$ GeV, and the interaction strength of XN force is 0.1 times that of NN force ($\delta = 0.1$). For this figure, we took the X^0 abundance to be $N_X/n_b = 1.7 \times 10^{-4}$ ($Y_X \equiv N_X/s = 1.5 \times 10^{-14}$), and its lifetime to be much longer than BBN time scale, i.e., $\tau_X \gg 200$ s. The X^0 reaction rates are given as described in the text, Sec. II. The dashed lines correspond to the abundances of normal nuclei in the standard BBN model.

capture by ^{4}He react with ^{7}Be [by $X(^7\mathrm{Be}, ^3\mathrm{He})^4\mathrm{He}_X$] and ^{7}Li [by $X(^7\mathrm{Li}, t)^4\mathrm{He}_X$]. The abundances of ^{7}Be and ^{7}Li thus decrease.

Figure 6 shows results of the abundances of normal and X nuclei as a function of temperature for Case 2 ($\delta = 0.2$). Parameters other than δ are the same as in Fig. 5. A clear difference from Case 1 is a complete capture of the X^0 particle by ^{4}He (see Sec. II B 2). Decreases in the abundances of ^{7}Be and ^{7}Li are, therefore, not seen. The

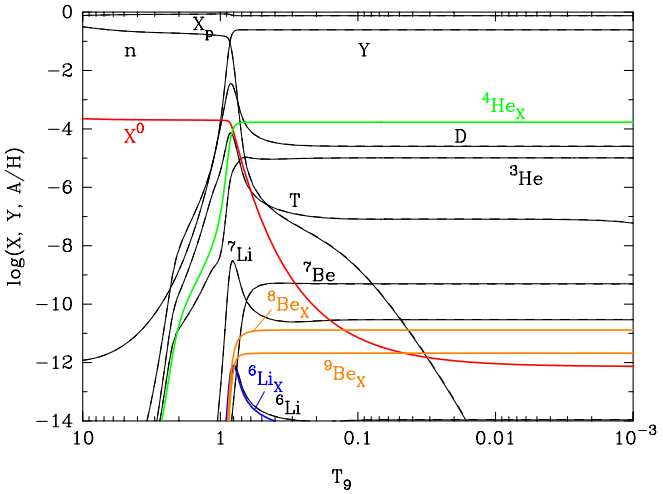

FIG. 6 (color online). Same as in Fig. 5 when the interaction strength of XN force is 0.2 times that of NN force ($\delta = 0.2$).

productions of $^6\mathrm{Li}_X$, $^8\mathrm{Be}_X$ and $^9\mathrm{Be}_X$ result following the $^4\mathrm{He}_X$ production similarly to Case 1.

B. Decrease in the primordial ^{7}Li abundance

Figure 7 shows abundances (solid curves) of ^{4}He (mass fraction), D, ^{3}He, ^{7}Li and ^{6}Li (by number relative to H) as a function of the baryon-to-photon ratio η or the baryon energy density $\Omega_B h^2$ of the universe. The solid curves are the calculated result in the X catalyzed BBN for Case 1, i.e., $(m_X, \delta, Y_X, \tau_X) = (100\ \mathrm{GeV}, 0.1, 1.5 \times 10^{-14}, \infty)$. The dashed curves are those in the SBBN. The boxes correspond to the adopted constraints on primordial abundances (see Appendix). The vertical stripe shows the 2σ limits on $\Omega_B h^2 = 0.02258^{+0.00057}_{-0.00056}$ provided by WMAP [59] for the ΛCDM + SZ + lens model.

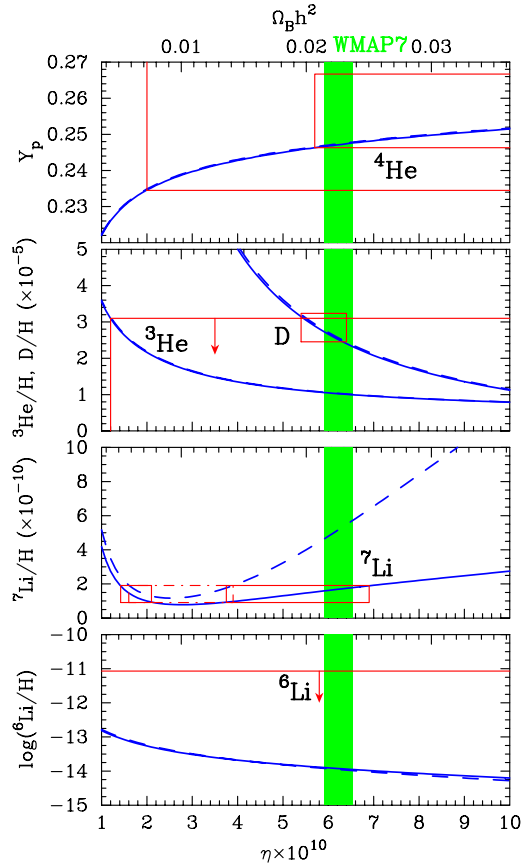

FIG. 7 (color online). Abundances of ^{4}He (mass fraction), D, ^{3}He, ^{7}Li and ^{6}Li (by number relative to H) as a function of the baryon-to-photon ratio η or the baryon energy density $\Omega_B h^2$ of the universe. The solid curves are the calculated results in the X catalyzed BBN for the case of $(m_X, \delta, Y_X, \tau_X) = (100\ \mathrm{GeV}, 0.1, 1.5 \times 10^{-14}, \infty)$, while the dashed curves are those in the standard BBN. There is virtually no difference between the dashed and solid curves for ^{4}He, D, ^{3}He, and ^{6}Li. The boxes represent the adopted abundance constraints from Refs. [132,133] for ^{4}He, [127] for D, [128] for ^{3}He, [54] for ^{7}Li, and [52] for ^{6}Li, respectively. The vertical stripe represents the 2σ $\Omega_B h^2$ limits provided by WMAP [59].

The decrease in the ^{7}Li abundance is found, while other nuclear abundances are not changed. A solution to the ^{7}Li problem is thus found in this model. One should note, however, that the abundance of $^9\mathrm{Be}_X$ could be higher than the adopted constraint on the primordial ^{9}Be abundance. For example, in Fig. 5, the final abundance of $^9\mathrm{Be}_X/\mathrm{H} \sim 2 \times 10^{-12}$ is shown. Effects of the decay of the X^0 particle inside X nuclei are not addressed in this paper. They should be studied in order to estimate fractions of $^9\mathrm{Be}_X$ which remain as ^{9}Be after the decay of X^0 particle.

C. Parameter region for Li reduction

If the strength of XN interaction is relatively weak as in the Cases 1 and 2 which we study in this paper, most strong reactions for the X^0 particle to get bound to nuclei would be nonradiative X^0-capture reactions, which are found important in the present model. We, however, note that efficiencies of the reactions are uncertain and that the present result is based on a rough assumption that the nonradiative cross sections have been set equal to the $^6\mathrm{Li}(n, \alpha)^3\mathrm{H}$ cross section excepting for the factor of reduced mass. Although effects of heavy X^0 particles during BBN were first studied recently [4], the possibility of X^0 capture reactions via nucleon emission has been mentioned in 1995 [2]. In order for these reactions to occur efficiently during BBN, reaction Q values need to be positive. The Q value of the reaction $X(A, b)B_X$ is given by

$$Q = \mathrm{BE}(B) + \mathrm{BE}(B_X) + \mathrm{BE}(b) - \mathrm{BE}(A), \qquad (31)$$

where BE(A), BE(B), and BE(b) are the binding energies of nuclei A, B, and b with respect to separated nucleons, respectively, and BE(B_X) is the binding energy of B_X with respect to separated B and X^0.

In Table IV, critical binding energies of B_X realizing $Q > 0$ are listed. We have taken data on binding energies of normal nuclei from Triangle Universities Nuclear Laboratory Nuclear Data Evaluation Project [116].

More important reactions than nucleon emissions in this X catalyzed BBN scenario are $X(^6\mathrm{Li}, d)^4\mathrm{He}_X$, $X(^7\mathrm{Li}, t)^4\mathrm{He}_X$, and $X(^7\mathrm{Be}, ^3\mathrm{He})^4\mathrm{He}_X$ [117]. Critical binding energies realizing $Q > 0$ for emissions of particles other than nucleons are also listed in Table IV.

Figure 8 shows contours in the parameter space (m_X, δ) for critical binding energies of X nuclei (thin and thick smooth curves) for the case of the Gaussian XN potential. Critical binding energies chosen for the plot are those of reactions, whose numbers are defined in Table IV: 2 (for n_X), 1 ($^1\mathrm{H}_X$) 3, 4 ($^2\mathrm{H}_X$), 5 ($^3\mathrm{H}_X$), 6 ($^3\mathrm{He}_X$), 14, 15, 16 ($^4\mathrm{He}_X$), 7 ($^5\mathrm{He}_X$), 8 ($^5\mathrm{Li}_X$), 10, 11 ($^6\mathrm{Li}_X$), 12 ($^6\mathrm{Be}_X$). Numbers attached to the contours indicate mass numbers of nuclides for elements which have more than two isotopes plotted. The contour of $Q = 0$ for the proton decay of $^6\mathrm{Be}_X$, i.e., $^6\mathrm{Be}_X(, 2p)^4\mathrm{He}_X$, is also shown as a thick solid line. Above the contours, reaction Q values are positive. Zigzag curves correspond to boundaries above which an excited state of $^4\mathrm{He}^*$ with $L = 1$ (upper line) and $^8\mathrm{Be}^*$ with $L = 1$ (lower) exist, respectively.

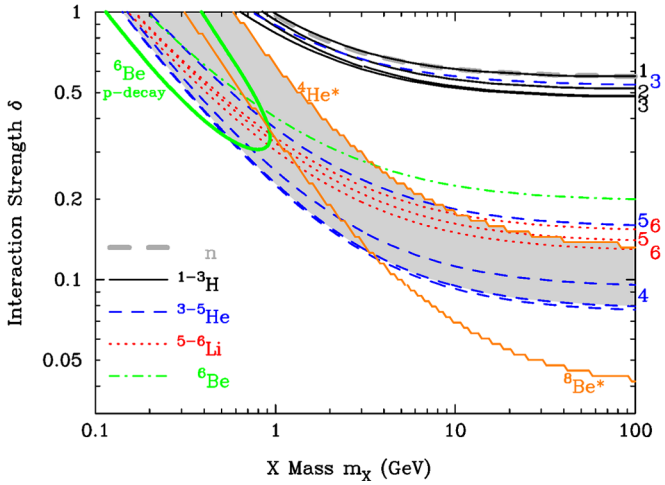

FIG. 8 (color online). Contours of binding energies between nuclei and an X^0 particle corresponding to $Q = 0$ of reactions (thin and thick smooth curves) for the case of the Gaussian XN potential. Numbers attached to the contours indicate mass numbers of nuclei. Above the contours, reaction Q values are positive (see text, Sec. III C). Zigzag curves correspond to boundaries above which an excited state of $^4\mathrm{He}^*$ (upper line) and $^8\mathrm{Be}^*$ (lower) exist, respectively. In the shaded region, the ^{7}Li problem can be resolved.

Figure 9 shows contours for the case of the square well XN potential corresponding to the same boundaries as in Fig. 8. The contours are very similar to those in Fig. 8 excepting for that of the proton decay of $^6\mathrm{Be}_X$. Although the difference in the contours of $^6\mathrm{Be}_X$ does not affect the BBN significantly, a realistic estimation of binding energies regarding all light nuclei are very important to obtain a realistic result of the catalyzed BBN.

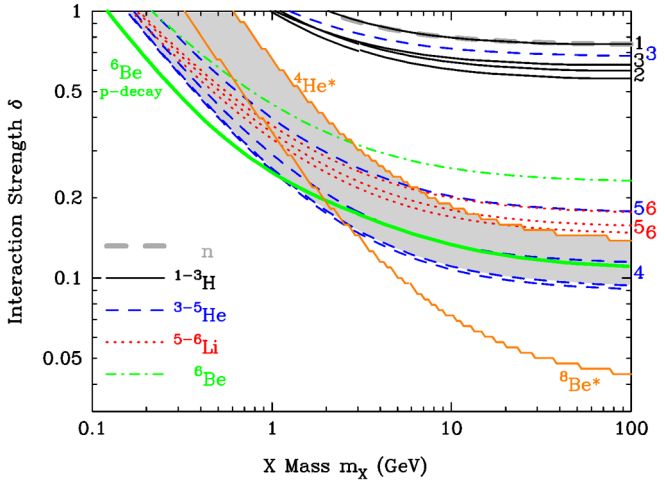

FIG. 9 (color online). Same as in Fig. 8 for the case of the square well XN potential.

We delineate the parameter region which might be responsible for a reduction of the primordial ^{7}Li abundance. The baryon-to-photon ratio is fixed to be $\eta = 6.225 \times 10^{-10}$ from WMAP determination [59]. In both Figs. 8 and 9, it is found that the contours of the boundaries for existences of $^4\mathrm{He}_X^*$ are above the contours of the reaction $X(^7\mathrm{Be}, ^3\mathrm{He})^4\mathrm{He}_X$ (the second lowest thin dashed lines). In the parameter region in right upper side from the curve of $^4\mathrm{He}_X^*$, free X^0 particles are captured onto ^{4}He at $T_9 \sim 1$ before they can react with ^{7}Be to reduce its abundance.

In the shaded region below that curve and above the curve of $X(^7\mathrm{Be}, ^3\mathrm{He})^4\mathrm{He}_X$, some amount of free X^0s possibly remain, and they can reduce the ^{7}Be abundance. This shaded region is, therefore, a possible parameter region where the ^{7}Li problem is solved. For a significant destruction of ^{7}Be, however, a relatively large value of initial abundance, i.e., $Y_X \sim O(10^{-14})$ is needed. Under the assumption of thermal freeze-out from equilibrium of the X^0 particle, the initial (relic) abundance is large if the annihilation cross section of X^0 particle is small [cf. Eq. (2)]. The required abundance may then realize in the scenario of substrongly interacting particle X^0 which has survived the annihilation due to its small interaction strength.

IV. CONCLUSIONS AND DISCUSSION

We have investigated effects on BBN of a long-lived strongly-interacting massive particle (SIMP) X^0 for different masses m_X and strengths of XN interaction, i.e., δ. Binding energies of bound states of nuclei and an X^0 particle, i.e., X nuclei, are calculated for two types of XN potentials, i.e., Gaussian and well types. It is shown that calculated binding energies are not largely dependent upon the potential shapes and are determined by the interaction strength at a given mass of X^0.

Evolutions of light element abundances are calculated as a function of the temperature for two specific cases of relatively weak interaction strengths. We found that ^{7}Be and ^{7}Li can be destroyed by the nuclear capture reactions of free X^0 particles. The reactions identified as destruction processes are $X(^7\mathrm{Be}, ^3\mathrm{He})^4\mathrm{He}_X$ and $X(^7\mathrm{Li}, t)^4\mathrm{He}_X$. We show that the lack of an excited state of $^4\mathrm{He}_X$ with a relative angular momentum $L = 1$ is essential for some fraction of the X^0 particles to escape capture by ^{4}He.

We suggest that the ^{7}Li problem could be solved based upon a network calculation of catalyzed BBN and found the parameter region in the (m_X, δ) plane where the ^{7}Li problem can be fixed.

We note that the results have been derived under the assumption that the X^0 particles do not change nuclear structure apart from sticking unaltered nuclei to the particles. This rough approximation is unlikely to be true especially in the case of relatively large strength of interaction since the XN potential is not much weaker than the NN potential and can not be neglected. More realistic estimations of wave functions and binding energies of X nuclei need to include such changes in nuclear structures with the use of three or more-body models. In the case of strongly bound ^{4}He, the binding energy of the ground state is 28 MeV, which is larger than binding energy of $^4\mathrm{He}_X$ with respect to separated ^{4}He and X^0. The effect of change in nuclear density caused by the existence of the X^0 then tends to be small for ^{4}He. The calculated binding energy of $^4\mathrm{He}_X$ and the cross section for radiative capture of X^0 on ^{4}He are, therefore, likely to be accurate. If the XN and XA potentials adopted in this paper describe well the real interaction, the main uncertainty in the BBN calculation would be in the estimations of nuclear reactions involving the X^0 particle. In this paper, the cross section of the most important reaction, i.e., $X(^7\mathrm{Be}, ^3\mathrm{He})^4\mathrm{He}_X$ was estimated only by analogy with $^6\mathrm{Li}(n, \alpha)^3\mathrm{H}$, and many other cross sections were also estimated using standard nuclear reaction rates. Radiative reaction cross sections were estimated approximately within the framework of two-body models. The rates should, however, be calculated in more rigorous quantum many-body models, not by the rough Born approximation, in order to derive realistic values. Although there might be errors in the calculated abundances in the X-catalyzed BBN of 1 order of magnitude or so, we argue at this moment that there is a possibility of ^{7}Li reduction in the BBN model including a long-lived sub-SIMP.

Effects of possible direct interactions of decay products of X^0 with the remaining nuclei A at the decay of X^0 in an X nucleus A_X are not taken into account yet. They should be studied in the future in order to better estimate final abundances of the light elements. In addition, nonthermal nucleosynthesis triggered by the decay process of the X^0 particle might change the abundances of normal nuclei if the energy injection by the decay were large enough. Recent studies suggest that the radiative decay could lead to the production of ^{6}Li to the level at most $\sim$10 times larger than that observed in MPHSs when the decay life is of the order of $\sim 10^8$–10^{12} s, which is associated with ^{3}He production [47]. The hadronic decay, on the other hand, can be a solution of both the lithium problems although that case gives somewhat elevated deuterium abundances [35,43].

For example, we assume that the mass and the initial abundance of the X are $m_X = 100$ GeV and $Y_X = 1.5 \times 10^{-14}$, respectively. The energy injection at the decay of the X into hadronic jets is constrained to be $\lesssim O(1$–100 GeV) if the lifetime is $\tau_X \gtrsim 10^2$ s through abundances of D, ^{4}He, ^{6}Li, and ^{3}He depending upon the lifetime (figure 38 of Ref. [32]). The energy injection into electromagnetic particles is, on the other hand, constrained to be $\lesssim O(10$ GeV) if the lifetime is $\tau_X \gtrsim 10^7$ s (figure 1 of Ref. [47]). This amount of energy injection tends to attain ^{6}Li production up to the observed level in MPHSs.

We summarize a present status of several models which have effects and thus leave observational signatures on

primordial light element abundances. In the BBN model catalyzed by a long-lived sub-SIMP studied in this paper, the abundance of ^{7}Li can be reduced below the level of SBBN prediction. In the BBN model catalyzed by a long-lived SIMP, the abundances of ^{9}Be or B can be high [4]. Moreover, the isotopic abundance ratio, i.e., $^{10}\mathrm{B}/^{11}\mathrm{B}$ can be high, which is never predicted in other scenarios for significant boron production [4]. In the BBN model catalyzed by a negatively charged massive particle (CHAMP), the ^{6}Li abundance can be high [5]. Only if the abundance of the CHAMP is more than (0.04–1) times as large as that of baryon [12,118], the ^{7}Li reduction can be possible [9]. A signature of CHAMP on ^{9}Be abundance has been estimated to be negligible [12,118] in the light of a rigorous quantum mechanical investigation [119]. The cosmological cosmic ray nucleosynthesis triggered by supernova explosion in an early epoch of the structure formation can produce ^{6}Li [120] as well as ^{9}Be and ^{10,11}B [89,121]. In baryon-inhomogeneous BBN models, the abundance of ^{9}Be can be higher than in the SBBN [122–126].

ACKNOWLEDGMENTS

This work is supported by Grant-in-Aid for JSPS Grant No. 21.6817 (Kusakabe) and Grant-in-Aid for Scientific Research from the Ministry of Education, Science, Sports, and Culture (MEXT), Japan, No. 22540267 and No. 21111006 (Kawasaki) and also by World Premier International Research Center Initiative (WPI Initiative), MEXT, Japan.

APPENDIX: CONSTRAINTS ON PRIMORDIAL LIGHT ELEMENT ABUNDANCES

We adopt constraints on primordial abundances as follows:

A mean value for the primordial deuterium abundance in Lyman-α absorption systems in the foreground of high redshift quasi-stellar objects has been estimated to be $\log(\mathrm{D/H}) = -4.55 \pm 0.03$ [127]. We adopt this value and a 2σ uncertainty, i.e.,

$$2.45 \times 10^{-5} < \mathrm{D/H} < 3.24 \times 10^{-5}. \quad \text{(A1)}$$

^{3}He abundances are measured in Galactic HII regions through the 8.665 GHz hyperfine transition of $^3\mathrm{He/H} = (1.9 \pm 0.6) \times 10^{-5}$ [128]. However, abundances in extragalactic objects have not been measured, and it is not known whether ^{3}He has increased or decreased through the course of stellar and galactic evolution [129,130]. ^{3}He is more resistant to the stellar burning than deuterium. Because the deuterium abundance does not appear to have decreased since the BBN epoch until the solar system formation [131], we do not assume a decrease in the ^{3}He abundance after BBN in amounts larger than the uncertainty in the abundance determination of Galactic HII regions. Although a constraint on the primordial ^{3}He abundance is rather weak considering its uncertainty, we take a 2σ upper limit from abundances in Galactic HII region as a rough guide, i.e.,

$$^3\mathrm{He/H} < 3.1 \times 10^{-5}. \quad \text{(A2)}$$

For the primordial helium abundance we adopt two different constraints, i.e, $Y = 0.2565 \pm 0.0051$ [132] and $Y = 0.2561 \pm 0.0108$ [133] both from observations of metal-poor extragalactic HII regions. We take 2σ limits of

$$0.2463 < Y < 0.2667 \quad \text{(IT10)}, \quad \text{(A3)}$$

and

$$0.2345 < Y < 0.2777 \quad \text{(AOS10)}. \quad \text{(A4)}$$

An upper limit on the ^{6}Li abundance is taken from the possible plateau abundance of $^6\mathrm{Li/H} = (7.1 \pm 0.7) \times 10^{-12}$ observed in metal-poor halo stars (MPHSs) [52]. A 2σ uncertainty is included, and we derive

$$^6\mathrm{Li/H} < 8.5 \times 10^{-12}. \quad \text{(A5)}$$

A limit on the ^{7}Li abundance is taken from observations of MPHSs, i.e., $^7\mathrm{Li/H} = (1.23^{+0.68}_{-0.32}) \times 10^{-10}$ (95% confidence limits) [54]. The adopted constraint on the ^{7}Li abundance is then

$$0.91 \times 10^{-10} < {}^7\mathrm{Li/H} < 1.91 \times 10^{-10}. \quad \text{(A6)}$$

Although we do not use constraints on abundances of nuclei with mass number $A \geq 9$ in this study, a primordial ^{9}Be may be related to the scenario (see Section III B). An upper limit on ^{9}Be abundance should be taken from the minimum abundances observed in MPHSs [134], i.e.,

$$^9\mathrm{Be/H} < 10^{-14}. \quad \text{(A7)}$$

[1] D. A. Dicus and V. L. Teplitz, Phys. Rev. Lett. **44**, 218 (1980).
[2] R. Plaga, Phys. Rev. D **51**, 6504 (1995).
[3] R. N. Mohapatra and V. L. Teplitz, Phys. Rev. Lett. **81**, 3079 (1998).
[4] M. Kusakabe, T. Kajino, T. Yoshida, and G. J. Mathews, Phys. Rev. D **80**, 103501 (2009).
[5] M. Pospelov, Phys. Rev. Lett. **98**, 231301 (2007).
[6] K. Kohri and F. Takayama, Phys. Rev. D **76**, 063507 (2007).

[7] R. H. Cyburt, J. R. Ellis, B. D. Fields, K. A. Olive, and V. C. Spanos, J. Cosmol. Astropart. Phys. 11 (2006) 014.
[8] K. Hamaguchi, T. Hatsuda, M. Kamimura, Y. Kino, and T. T. Yanagida, Phys. Lett. B **650**, 268 (2007).
[9] C. Bird, K. Koopmans, and M. Pospelov, Phys. Rev. D **78**, 083010 (2008).
[10] M. Kusakabe, T. Kajino, R. N. Boyd, T. Yoshida, and G. J. Mathews, Phys. Rev. D **76**, 121302 (2007).
[11] M. Kusakabe, T. Kajino, R. N. Boyd, T. Yoshida, and G. J. Mathews, Astrophys. J. **680**, 846 (2008).
[12] M. Kusakabe, T. Kajino, T. Yoshida, and G. J. Mathews, Phys. Rev. D **81**, 083521 (2010).
[13] K. Jedamzik, Phys. Rev. D **77**, 063524 (2008).
[14] K. Jedamzik, J. Cosmol. Astropart. Phys. 03 (2008) 008.
[15] M. Kamimura, Y. Kino, and E. Hiyama, Prog. Theor. Phys. **121**, 1059 (2009).
[16] M. Pospelov, arXiv:0712.0647.
[17] M. Kawasaki, K. Kohri, and T. Moroi, Phys. Lett. B **649**, 436 (2007).
[18] T. Jittoh *et al.*, Phys. Rev. D **76**, 125023 (2007).
[19] T. Jittoh *et al.*, Phys. Rev. D **78**, 055007 (2008).
[20] T. Jittoh *et al.*, Phys. Rev. D **82**, 115030 (2010).
[21] M. Pospelov, J. Pradler, and F. D. Steffen, J. Cosmol. Astropart. Phys. 11 (2008) 020.
[22] M. Y. Khlopov and C. Kouvaris, Phys. Rev. D **77**, 065002 (2008).
[23] J. R. Ellis, D. V. Nanopoulos, and S. Sarkar, Nucl. Phys. **B259**, 175 (1985).
[24] R. H. Cyburt, J. R. Ellis, B. D. Fields, and K. A. Olive, Phys. Rev. D **67**, 103521 (2003).
[25] J. R. Ellis, K. A. Olive, and E. Vangioni, Phys. Lett. B **619**, 30 (2005).
[26] N. Terasawa, M. Kawasaki, and K. Sato, Nucl. Phys. **B302**, 697 (1988).
[27] M. Kawasaki *et al.*, Nucl. Phys. **B419**, 105 (1994).
[28] M. Kawasaki and T. Moroi, Prog. Theor. Phys. **93**, 879 (1995).
[29] E. Holtmann, M. Kawasaki, and T. Moroi, Phys. Rev. Lett. **77**, 3712 (1996).
[30] M. Kawasaki, K. Kohri, and T. Moroi, Phys. Rev. D **63**, 103502 (2001).
[31] M. Kawasaki, K. Kohri, and T. Moroi, Phys. Lett. B **625**, 7 (2005).
[32] M. Kawasaki, K. Kohri, and T. Moroi, Phys. Rev. D **71**, 083502 (2005).
[33] T. Kanzaki, M. Kawasaki, K. Kohri, and T. Moroi, Phys. Rev. D **75**, 025011 (2007).
[34] M. Kawasaki, K. Kohri, T. Moroi, and A. Yotsuyanagi, Phys. Rev. D **78**, 065011 (2008).
[35] D. Cumberbatch *et al.*, Phys. Rev. D **76**, 123005 (2007).
[36] M. H. Reno and D. Seckel, Phys. Rev. D **37**, 3441 (1988).
[37] S. Dimopoulos, R. Esmailzadeh, L. J. Hall, and G. D. Starkman, Astrophys. J. **330**, 545 (1988).
[38] S. Dimopoulos, R. Esmailzadeh, L. J. Hall, and G. D. Starkman, Phys. Rev. Lett. **60**, 7 (1988).
[39] S. Dimopoulos, R. Esmailzadeh, L. J. Hall, and G. D. Starkman, Nucl. Phys. **B311**, 699 (1989).
[40] M. Y. Khlopov, Y. L. Levitan, E. V. Sedelnikov, and I. M. Sobol, Phys. At. Nucl. **57**, 1393 (1994).
[41] E. V. Sedelnikov, S. S. Filippov, and M. Y. Khlopov, Phys. At. Nucl. **58**, 235 (1995).
[42] K. Jedamzik, Phys. Rev. Lett. **84**, 3248 (2000).
[43] K. Jedamzik, Phys. Rev. D **70**, 063524 (2004).
[44] K. Jedamzik, Phys. Rev. D **70**, 083510 (2004).
[45] K. Jedamzik, K.-Y. Choi, L. Roszkowski, and R. Ruiz de Austri, J. Cosmol. Astropart. Phys. 07 (2006) 007.
[46] K. Jedamzik, Phys. Rev. D **74**, 103509 (2006).
[47] M. Kusakabe, T. Kajino, and G. J. Mathews, Phys. Rev. D **74**, 023526 (2006).
[48] M. Kusakabe *et al.*, Phys. Rev. D **79**, 123513 (2009).
[49] M. Pospelov and J. Pradler, Phys. Rev. D **82**, 103514 (2010).
[50] M. Pospelov and J. Pradler, arXiv:1010.4079.
[51] J. Melendez and I. Ramirez, Astrophys. J. **615**, L33 (2004).
[52] M. Asplund, D. L. Lambert, P. E. Nissen, F. Primas, and V. V. Smith, Astrophys. J. **644**, 229 (2006).
[53] F. Spite and M. Spite, Astron. Astrophys. **115**, 357 (1982).
[54] S. G. Ryan, T. C. Beers, K. A. Olive, B. D. Fields, and J. E. Norris, Astrophys. J. **530**, L57 (2000).
[55] P. Bonifacio, P. Molaro, T. Sivarani, R. Cayrel, M. Spite, F. Spite, B. Plez, J. Andersen, B. Barbuy, T. C. Beers *et al.*, Astron. Astrophys. **462**, 851 (2007).
[56] J. R. Shi, T. Gehren, H. W. Zhang, J. L. Zeng, and G. Zhao, Astron. Astrophys. **465**, 587 (2007).
[57] W. Aoki *et al.*, Astrophys. J. **698**, 1803 (2009).
[58] R. H. Cyburt, B. D. Fields, and K. A. Olive, J. Cosmol. Astropart. Phys. 11 (2008) 012.
[59] D. Larson *et al.*, Astrophys. J. Suppl. Ser. **192**, 16 (2011).
[60] O. Richard, G. Michaud, and J. Richer, Astrophys. J. **619**, 538 (2005).
[61] A. J. Korn *et al.*, Nature (London) **442**, 657 (2006).
[62] K. Lind, F. Primas, C. Charbonnel, F. Grundahl, and M. Asplund, Astron. Astrophys. **503**, 545 (2009).
[63] Recently, a new measurement of the cross section of radiative capture by deuteron and the ^{6}Li abundance predicted based upon the result have been reported [64].
[64] F. Hammache *et al.*, Phys. Rev. C **82**, 065803 (2010).
[65] R. Cayrel *et al.*, Astron. Astrophys. **473**, L37 (2007).
[66] M. Steffen, R. Cayrel, P. Bonifacio, H. G. Ludwig, and E. Caffau, arXiv:0910.5917.
[67] N. Prantzos, Astron. Astrophys. **448**, 665 (2006).
[68] $[A/H] = \log(A/H) - \log(A/H)_\odot$ is the number ratio of nuclide A to H measured in a logarithmic scale normalized to the solar value.
[69] R. N. Boyd, C. R. Brune, G. M. Fuller, and C. J. Smith, Phys. Rev. D **82**, 105005 (2010).
[70] R. H. Cyburt and M. Pospelov, arXiv:0906.4373.
[71] N. Chakraborty, B. D. Fields, and K. A. Olive, arXiv:1011.0722.
[72] N. Arkani-Hamed and S. Dimopoulos, J. High Energy Phys. 06 (2005) 073.
[73] N. Arkani-Hamed, S. Dimopoulos, G. F. Giudice, and A. Romanino, Nucl. Phys. **B709**, 3 (2005).
[74] S. Raby, Phys. Lett. B **422**, 158 (1998).
[75] S. Shirai, M. Yamazaki, and K. Yonekura, J. High Energy Phys. 06 (2010) 056.
[76] L. Covi, M. Olechowski, S. Pokorski, K. Turzynski, and J. D. Wells, J. High Energy Phys. 01 (2011) 033.
[77] U. Sarid and S. D. Thomas, Phys. Rev. Lett. **85**, 1178 (2000).

[78] J. Hisano, K. Nakayama, S. Sugiyama, T. Takesako, and M. Yamanaka, Phys. Lett. B **691**, 46 (2010).
[79] K. Nakayama, F. Takahashi, and T. T. Yanagida, arXiv:1010.5693.
[80] J. Kang, M. A. Luty, and S. Nasri, J. High Energy Phys. 09 (2008) 086.
[81] H. Baer, K.-m. Cheung, and J. F. Gunion, Phys. Rev. D **59**, 075002 (1999).
[82] E. W. Kolb and M. S. Turner, *The Early Universe* (Addison-Wesley, Reading, MA, 1990).
[83] S. Wolfram, Phys. Lett. B **82**, 65 (1979).
[84] C. B. Dover, T. K. Gaisser, and G. Steigman, Phys. Rev. Lett. **42**, 1117 (1979).
[85] G. D. Starkman, A. Gould, R. Esmailzadeh, and S. Dimopoulos, Phys. Rev. D **41**, 3594 (1990).
[86] K. Nakamura and Particle Data Group, J. Phys. G **37**, 075021 (2010).
[87] N. Prantzos, M. Casse, and E. Vangioni-Flam, Astrophys. J. **403**, 630 (1993).
[88] R. Ramaty, B. Kozlovsky, R. E. Lingenfelter, and H. Reeves, Astrophys. J. **488**, 730 (1997).
[89] M. Kusakabe, Astrophys. J. **681**, 18 (2008).
[90] S. E. Woosley and T. A. Weaver, Astrophys. J. Suppl. Ser. **101**, 181 (1995).
[91] T. Yoshida, T. Kajino, and D. H. Hartmann, Phys. Rev. Lett. **94**, 231101 (2005).
[92] These parameters have been adjusted to fit the deuteron binding energy and low-energy triplet-even proton-neutron scattering phase shifts [93,94].
[93] M. Yahiro, Y. Iseri, H. Kameyama, M. Kamimura, and M. Kawai, Prog. Theor. Phys. Suppl. **89**, 32 (1986).
[94] N. Austern *et al.*, Phys. Rep. **154**, 125 (1987).
[95] This value is an example which leads to the binding energy of deuteron when another parameter is fixed to be $v_{0w} = -25.5$ MeV.
[96] E. Hiyama, M. Kamimura, T. Motoba, T. Yamada, and Y. Yamamoto, Phys. Rev. C **66**, 024007 (2002).
[97] E. Hiyama, Y. Kino, and M. Kamimura, Prog. Part. Nucl. Phys. **51**, 223 (2003).
[98] J. Martorell, D. W. L. Sprung, and D. C. Zheng, Phys. Rev. C **51**, 1127 (1995).
[99] A. Amroun *et al.*, Nucl. Phys. A **579**, 596 (1994).
[100] I. Tanihata *et al.*, Phys. Lett. B **206**, 592 (1988).
[101] M. Fukuda, M. Mihara, T. Fukao, S. Fukuda, M. Ishihara, S. Ito, T. Kobayashi, K. Matsuta, T. Minamisono, S. Momota *et al.*, Nucl. Phys. A **656**, 209 (1999).
[102] C. Angulo *et al.*, Nucl. Phys. A **656**, 3 (1999).
[103] R. N. Boyd, *An Introduction to Nuclear Astrophysics* (University of Chicago, Chicago, 2008).
[104] W. A. Fowler, G. R. Caughlan, and B. A. Zimmerman, Annu. Rev. Astron. Astrophys. **5**, 525 (1967).
[105] G. R. Caughlan and W. A. Fowler, At. Data Nucl. Data Tables **40**, 283 (1988).
[106] M. Sowerby, J. Nucl. Energy **24**, 323 (1970).
[107] The $^6\mathrm{Be}_X$ nucleus produced in this reaction pathway immediately p decays into $^4\mathrm{He}_X$ and two protons.
[108] C. A. Bertulani, Comput. Phys. Commun. **156**, 123 (2003).
[109] G. G. Simon, C. Schmitt, and V. H. Walther, Nucl. Phys. A **364**, 285 (1981).
[110] D. R. Tilley *et al.*, Nucl. Phys. A **708**, 3 (2002).
[111] L. Kawano, *Recon Technical Report N*, 92, 25163 (NASA STI Program, Hanover, MD, 1992).
[112] M. S. Smith, L. H. Kawano, and R. A. Malaney, Astrophys. J. Suppl. Ser. **85**, 219 (1993).
[113] P. Descouvemont, A. Adahchour, C. Angulo, A. Coc, and E. Vangioni-Flam, At. Data Nucl. Data Tables **88**, 203 (2004).
[114] G. J. Mathews, T. Kajino, and T. Shima, Phys. Rev. D **71**, 021302 (2005).
[115] This reaction can be efficient since the reaction Q-value of $X(^7\mathrm{Li}, t)^4\mathrm{He}_X$ is very small (see Table II).
[116] http://www.tunl.duke.edu/nucldata/index.shtml.
[117] The reaction rates and related information of $^4\mathrm{He}_X(d, ^6\mathrm{Li})X$, $^4\mathrm{He}_X(t, ^7\mathrm{Li})X$ and $^4\mathrm{He}_X(^3\mathrm{He}, ^7\mathrm{Be})X$ in the case of leptonic X^- particle can be found in Refs. [8,15].
[118] M. Kusakabe, T. Kajino, and G. J. Mathews, Proceedings in the Open Access Journal of Physics: Conference Series, (IOP Publishing, Bristol, England, to be published).
[119] M. Kamimura, Y. Kino, and E. Hiyama, in *American Institute of Physics Conference Series*, edited by H. Susa, M. Arnould, S. Gales, T. Motobayashi, C. Scheidenberger, and H. Utsunomiya, American Institute of Physics Conference Series Vol. 1238 (American Institute of Physics, Melville, NY, 2010), pp. 139–144.
[120] E. Rollinde, E. Vangioni, and K. A. Olive, Astrophys. J. **651**, 658 (2006).
[121] E. Rollinde, D. Maurin, E. Vangioni, K. A. Olive, and S. Inoue, Astrophys. J. **673**, 676 (2008).
[122] R. N. Boyd and T. Kajino, Astrophys. J. **336**, L55 (1989).
[123] T. Kajino and R. N. Boyd, Astrophys. J. **359**, 267 (1990).
[124] T. Kajino, G. J. Mathews, and G. M. Fuller, Astrophys. J. **364**, 7 (1990).
[125] A. Coc, P. Delbourgo-Salvador, F. de Oliveira, P. Aguer, S. Barhoumi, G. Bogaert, J. Kiener, A. Lafebvre, and J. P. Thibaud, Astrophys. J. **402**, 62 (1993).
[126] M. Orito, T. Kajino, R. N. Boyd, and G. J. Mathews, Astrophys. J. **488**, 515 (1997).
[127] M. Pettini, B. J. Zych, M. T. Murphy, A. Lewis, and C. C. Steidel Mon. Not. R. Astron. Soc. **391**, 1499 (2008).
[128] T. M. Bania, R. T. Rood, and D. S. Balser, Nature (London) **415**, 54 (2002).
[129] C. Chiappini, A. Renda, and F. Matteucci, Astron. Astrophys. **395**, 789 (2002).
[130] E. Vangioni-Flam, K. A. Olive, B. D. Fields, and M. Casse, Astrophys. J. **585**, 611 (2003).
[131] K. Lodders, Astrophys. J. **591**, 1220 (2003).
[132] Y. I. Izotov and T. X. Thuan, Astrophys. J. **710**, L67 (2010).
[133] E. Aver, K. A. Olive, and E. D. Skillman, J. Cosmol. Astropart. Phys. 05 (2010) 003.
[134] H. Ito, W. Aoki, S. Honda, and T. C. Beers, Astrophys. J. **698**, L37 (2009).